SHIRSHOV INSTITUTE OF OCEANOLOGY

CRUISE REPORT No. 50

RV *AKADEMIK SERGEY VAVILOVH* CRUISE 50 7 August – 12 September 2020

North Atlantic Repeat Hydrography of WOCE section along 59.5 N and sill sections between Greenland - Iceland - Faroe Islands and Shetlands

Principal Scientist **S. Gladyshev**[1]

2021

Shirshov Institute of Oceanology
36 Nakhimovskii prospect
Moscow 117997 RUSSIA
Tel: +7(495) 719 0255 Fax: +7(499) 124 6342
Email :sgladyshev@ocean.ru

[1]**Shirshov Institute of Oceanology**

DOCUMENT DATA SHEET

AUTHOR	***PUBLICATION DATE***
GLADYSHEV, S	2021

TITLE

RV ***Akademik Sergey Vavilov*** Cruise 50 , 7 August – 12 September 2020.

REFERENCE

Shirshov Institute of Oceanology, Akademik Sergey Vavilov Cruise Report, No. 50, 70pp. tables & figs.

ABSTRACT

RV ***Akademik Sergey Vavilov*** Cruise 50 was a contribution to the Russian CLIVAR and State Research Programmes. CTD sections were designed to enable the ocean circulation in the Subpolar Gyre of the North Atlantic to be mapped and in particular the pathways of the North Atlantic, Irminger and East Greenland Currents within the region to be determined. The main goal is to continue annual monitoring of the North Atlantic large-scale circulation and climate changes in the North Atlantic started in 1997. The sections over North Atlantic sills between Greenland - Iceland - Faroe Islands and Shetlands were carried out to estimate variability of the meridional fluxes and water mass exchange between the North Atlantic and the Arctic Ocean. The quiasimeridional sections along Reykjanes Ridge and south of Faroe Islands were made to close water balance between the main deep North Atlantic basins.

KEYWORDS

CRUISE 50 2020, *AKADEMIK SERGEY VVILOV,* **CLIVAR, TRANSATLANTIC SECTION, EAST GREENLAND CURRENT, IRMINGER BASIN, NORTH ATLANTIC SUBPOLAR GYRE, CTD OBSERVATIONS, LADCP, VMADCP, SILLS, REYKJANES RIDGE**

ISSUING ORGANISATION

Shirshov Institute of Oceanology
36 Nakhimovskii prospect
Moscow 117997 RUSSIA

Director: Dr. Alexey Sokov

Copies of this report are available from: **Marine Expedition Centre,** Tel: +7(495)7190255 Fax: +7(499)124 6342

Email: sgladyshev@ocean.ru

Contents

Scientific Personnel

GLADYSHEV, S.	Principal Scientist	Shirshov	
GLADYSHEV, V.	Chief of CTD Group	Shirshov	
ZAPOTYL'KO, V.	CTD, LADCP	Shirshov	
LUKASHIN, S.	Winch	Shirshov	Atlantic Branch
PYATAKOV, V.	Sampling	Shirshov	Atlantic Branch
VEREZEMSKAYA, P	CTD, LADCP	Shirshov	
DROZD, I.	CTD, LADCP	MGU	
RYBIN, A.	LADCP, Sampling	MFTI	
ZHDANOV, I.	Sampling	Shirshov	
POPOV, M.	Sampling	MFTI	
YASINSKII, V.	CTD, LADCP	Shirshov	
KOLOKOLOVA, A	Chief of Chemistry Group	Shirshov	
MURATOVA, A.	Oxygen	BFU	
GAVRIKOV, A	Chief of Wave Group	Shirshov	
TILININA, N.	Radar Operator	Shirshov	
SHARMAR, V.	Buoy launch	Shirshov	
IVONIN, D.	Data Processing	Shirshov	
SALAVATOVA, L.	Radar Operator	MFTI	

1. CRUISE NARRATIVE

1.1 Cruise Details

Expedition Designation: R/V ***Akademik Sergry Vavilov*** Cruise 50, RUSSIA CLIVAR

Principal Scientist: Dr. Sergey V. Gladyshev (Shirshov).

Ship: RV ***Akademik Sergey Vavilov.***

Ports of Call: Kaliningrad (Russia) to Kaliningrad (Russia).

Cruise Dates: 7th August to 12th September 2020.

1.2 Cruise Summary

1.2.1 Cruise Track and Stations

The cruise track with station positions is shown in **Fig. l**. Only small volume samples were taken, details are listed in **Table 1**.

1.2.2. Equipment

The principal instruments used during the cruise were a SBE 9P-1267 CTD with dual temperature and conductivity sensors (SBE 3 SN 03P6082, SBE 4 SN 044580, SBE 3 SN 03P6088, SBE 4 SN 044581), oxygen sensor (SBE 43, SN 430699), fluorimeter-turbidity sensor (WET Labs, SN 4237), Benthos altimeter model PSA-916, LADCP WHS-300 kHz down-looking (S/N 6393), LADCP WHS-300 kHz up-looking (S/N 14151). These were mounted together with a multisampler Carousel SBE 32 equipped with 22 5-litre Niskin bottles. Upon recovery, each bottle was sampled in turn for dissolved oxygen. All sampling was done on deck. Currents were measured using vessel mounted ADCP (VM ADCP) TRDI OS75 kHz installed at the central point of the ship hall.

3D navigation information was provided by a Trimble SPS 461 - Modular GPS receiver and GPS antenna Trimble GA830 GNSS/MSS/Beacon together with MRU 3 (Kongsberg) and every second was recorded on the PC. Additional measurements were made with an EA600 12 kHz and AIRMAR Weather Station 150WX.

1.2.3 Sampling

Nominal depths sampled were: bottom, 3100, 3000, 2750, 2500, 2250, 2000, 1750, 1500, 1250, 1100, 1000, 900, 800, 700, 600, 500, 400, 300, 200, 150, 100, 50, 30, 20, 10 m. On deep casts fewer shallow and intermediate bottles were fired. The actual bottle depths are shown in **Fig. 2**.

1.2.4 Number of Stations Occupied

197 stations (197 casts) were occupied during the cruise along transatlantic section along 59.5 N, along Reykjanes Ridge crest, along North-Atlantic sills, and south of the Faroe Islands (**Fig. l**).

1.3 Scientific Objectives

The cruise objectives were to:

1. To complete the CTD section from Scotland to Greenland along 59.5 N.
2. To complete the CTD section along Reykjanes Ridge from 56º N to Iceland shelf.
3. To carry out the CTD sections along Greenland Scotland Ridge
4. To complete quasi meridional section between Faroe Islands and 59.5 N.

1.4 Narrative

1.4.1 Introduction

The Meridional overturning circulation (MOC) in the North Atlantic is one of the main drivers of the widely known global oceanic "conveyor belt" – an important element of the Earth's climate system [e.g., van Aken, 2007]. Warm upper-ocean waters transported northward by the North Atlantic Current release heat to the atmosphere, gain density due to cooling and eventually sink in the subpolar North Atlantic and adjacent Arctic seas thereby generating the return southward flow of colder waters at depths (**Fig. 3**) [Dickson and Brown, 1994; Koltermann et al., 1999]. Temporal variability of the large-scale circulation and associated heat transport in the subpolar North Atlantic is one of the principal factors behind the high-latitude climate anomalies in the Northern Hemisphere.

Progress in understanding the causes of the ongoing climate change and forecasting climate variability in the Arctic and over European part of Russia for the next decades require

reliable observation-based estimates of the variability of the North Atlantic circulation and the Atlantic–Arctic heat and freshwater fluxes, as well as elucidation of the underlying mechanisms. In a number of recent studies, radical changes in the thermohaline regime and large-scale circulation in the Atlantic Ocean have been suggested to occur under global warming. For instance, the long-term freshening of the subpolar North Atlantic deep waters since the mid-1960s [Dickson et al., 2002] has been (cautiously) attributed to climate change-related factors [Curry et al., 2003; Hansen et al., 2004]. Hypothetically, under global warming, an increased evaporation in the tropics and increased precipitation at high latitudes, coupled with an intensified melting of Arctic ice, lead to the upper-ocean freshening in the regions of deep water formation and, hence, to the deep water freshening in the Atlantic Ocean. At the same time, milder winters along with the upper-ocean freshening lead to a decrease in the deep water production rates, which results in slowing of the Atlantic Meridional Overturning Circulation [e.g., Hansen et al., 2004; Bryden et al., 2005].

To better understand the past and present changes in the ocean-atmosphere dynamical system, as well as their causes and consequences, data on the full-depth oceanic variability are needed. An indispensable effective tool for assessing the large-scale circulation and thermohaline changes in the deep ocean and investigating mechanisms governing these changes are repeated full-depth transoceanic observations.

Since 1997, the P.P. Shirshov Institute of Oceanology has carried out the long-term monitoring of the North Atlantic circulation and water mass properties in the 59.5°N hydrographic section between Cape Farewell (Greenland) and Scotland (**Fig. 3**). Since 2002, the section has been repeated yearly on board the Russian research vessels, providing high precision data on temperature, salinity, oxygen and nutrients concentrations, and current velocities in the entire water column – "from shore to shore", from the sea surface to the bottom. In addition to annual repeat measurements at 59.5°N, the P.P. Shirshov Institute of Oceanology started full-depth repeat observations of the oceanic exchange between the Atlantic and Arctic oceans across the straits between Greenland, Iceland, Faeroe and Shetland Islands in 2011 (**Fig. 3**). The full-depth observations – of the same oceanic quantities as at 59.5°N – are performed in the straits from research vessels once a year. Based on the unique data set thus collected, a number of fundamental findings have already been achieved. Below, we briefly summarize the main subjects and results of our research.

The 59.5°N transatlantic section (**Fig. 3**) was designed for monitoring the large-scale circulation and thermohaline / chemical properties of oceanic waters at the northern periphery of the NA – the region where the warm upper-ocean waters are transformed by deep convection and mixing into the colder intermediate and deep waters – the Labrador Sea Water (LSW), Iceland Scotland Overflow Water (ISOW) and Denmark Strait Overflow Water (DSOW) (**Fig. 3**) – transported southward in the lower limb of the Atlantic MOC. Hydrographic data collected at 59.5°N along with those obtained within the framework of the kindred projects, primarily the French OVIDE (http://www.ifremer.fr/lpo/ovide), and historical data sets have been used for studying the dense water production [Falina et al., 2007; Falina et al., 2012], decadal temperature and salinity changes in the intermediate–deep water column [Sarafanov et al., 2007; Sarafanov et al., 2008; Sarafanov et al., 2010b, Gladyshev et al., 2016, Gladyshev et al., 2018], causes of these changes [Sarafanov, 2009; Sarafanov et al., 2010b], the mean state [Sarafanov et al, 2012] and long-term variability of the large-scale circulation in the region [Sarafanov et al., 2009; Sarafanov et al, 2010a; Våge et al., 2011].

1.4.2 Deep convection in the Irminger Sea

The oxygen data collected in 1997 in the northern North Atlantic in several sections ending nearby the southern tip of Greenland provided the observation-based support for the hypothesis [Pickart et al., 2003] that winter convection in the Irminger Sea may penetrate deep into the LSW layer (1000 – 2000 m) thus causing local renewal of this water mass. A separate lateral maximum of oxygen concentrations in the deep LSW layer was detected east of Cape Farewell (59.5°N, 36–40°W): the concentrations increased (by ~0.1 ml/l) from the Labrador Sea eastern edge toward the Irminger Sea (**Fig. 4**) rather than the reverse, as would be expected if LSW observed in the Irminger Sea interior in 1997 were solely of advective origin [Falina et al., 2007].

The section along 59.5 N crosses the northernmost convection site in the Irminger Sea. The northernmost LSW is characterized by relatively high temperature and salinity because of contribution of the Irminger Current along Greenland. Its thermohaline variability in 21 century is shown by Gladyshev et al., 2016. The decadal LSW warming and salinification reversed in 2012. Strong and continuous cooling and freshening occurred after 2015 when anomalous convection developed in the Irminger Sea [Gladyshev et al., 2016, Gladyshev et al., 2019].

1.4.3. Reversal of the deep-water freshening

The LSW and Nordic Seas overflow-derived deep waters, ISOW and DSOW, freshened in the northern North Atlantic during the last three–four decades of the 20th century [Dickson et al., 2002]. Between the 1960s and 1990s, the water column in the region freshened on average by about 0.03 [Curry et al., 2003].

The long-term freshening reversed in the mid-1990s [Sarafanov et al., 2007; Sarafanov et al., 2008; Sarafanov et al., 2010b]. The salinification (and warming) of the intermediate and deep waters since the mid-1990s (**Fig. 5**) was much more intense than the preceding freshening. Over nearly a decade (1997–2006), temperature / salinity in the intermediate–deep water column ($\sigma_0 \geq 27.45$, depths > 500–1000 m) at 59.5°N increased by ~0.3°C / 0.03–0.04 [Sarafanov et al., 2008].

In the Irminger Sea, the long-term freshening in the deep water column (σ_0>27.80, depths > ~2000 m) reversed in the early 2000s [Sarafanov et al., 2010b]. The observed freshening reversal was a lagged consequence of the persistent ISOW salinification that occurred upstream, in the Iceland Basin, after 1996 due to salinification of the northeast Atlantic waters entrained into the overflow. It was demonstrated [Sarafanov et al., 2010b] that the entrainment salinity increase was associated with the North Atlantic Oscillation (NAO)-induced weakening and contraction of the Subpolar Gyre and corresponding northwestward advance of subtropical waters that followed the NAO decline in the mid-1990s and continued through the mid-2000s. Remarkably, the deep water freshening reversal was not related to changes in the overflow water salinity.

1.4.4. Deep-ocean salinity changes and the NAO

Close relationship between the thermohaline properties of the northern North Atlantic intermediate and deep waters and the winter NAO index on a decadal time scale ($r^2 \approx 0.65$, 1950s–2000s, **Fig. 6b** and **6c**) was revealed [Sarafanov, 2009] from the observation-based salinity time series for LSW in the Labrador Sea [Yashayaev, 2007] and ISOW in the Iceland basin [Boessenkool et al., 2007; Sarafanov et al., 2007]. Persistent NAO decline (amplification) leads to warming and salinification (cooling and freshening) in the intermediate–deep water column.

An explanation for the close link between the NAO and the coherent decadal changes in the intermediate and deep water properties in the region was proposed [Sarafanov, 2009]. The two factors dominate this link (**Fig. 6d**): (i) intensity of convection in the Labrador Sea controlling injection of relatively cold fresh waters into the intermediate layer and (ii) zonal extent of the Subpolar Gyre that regulates the relative contributions of cold fresh subpolar waters and warm saline subtropical waters to the entrainment into the Norwegian Sea overflow south of the Iceland–Scotland Ridge and to the Atlantic inflow to the Nordic Seas. These factors act in phase leading to the observed coherent thermohaline changes in the intermediate–deep water column.

Due to weakening of the surface forcing associated with the NAO transition into neutral to low phase (1950s to mid-1960s, mid-1990s to mid-2000s), convection in the Labrador Sea weakens diminishing cold fresh water penetration into the intermediate layer. This results in warming and salinification at the intermediate depths in the Subpolar Gyre. Concurrently, the Subpolar Gyre contracts allowing northward advance of warm saline upper-ocean and intermediate subtropical waters in the northeastern North Atlantic. Northward progression of subtropical waters increases temperature and salinity at the upper intermediate levels and, correspondingly, increases temperature and salinity of the northeast Atlantic waters entrained into the Iceland–Scotland overflow along its pathway to the deep Iceland basin. As a result, temperature and salinity at the deep levels increase. The contrary changes – intensification of deep convection in the Labrador Sea and expansion of the Subpolar Gyre – caused by amplifying surface forcing (mid-1960s to mid-1990s) lead to cooling and freshening at the intermediate–deep levels. Additionally, under high-NAO conditions, deep convection may occur in the Irminger Sea potentially contributing to cooling and freshening at the intermediate (LSW) levels. The two regimes of convection and large-scale circulation corresponding to stronger (early 1990s) and weaker (mid-1960s, mid-2000s) NAO-related atmospheric forcing are schematically visualized in **Fig. 7**.

1.4.5 Deep-ocean salinity changes and climate change

There are increasing concerns that in the warmer climate, the MOC may substantially decline due to a decrease in the convective activity in the northern North Atlantic and Nordic Seas [e.g., Meehl et al., 2007]. The long-term freshening in the Nordic Seas and freshening of

the northern North Atlantic deep waters in the 1960s–1990s have been considered as a likely indicator or precursor of the dramatic change in the MOC [e.g., Hansen et al., 2004]. The freshening has been attributed to a combination of factors potentially associated with the global warming: the increasing ice melt and net precipitation at high latitudes [e.g., Curry et al., 2003]. A probable causality between the climate change and the decreasing North Atlantic deep water salinity has supported the concerns and unfavorable predictions, thus 'warming up' the reasonable scientific debate on climate change and overblown speculations in media.

Despite the long-term increase in freshwater input to the Arctic, freshening in the northern North Atlantic had reversed in the mid-1990s, as we demonstrated above. This reversal forces us to revise the hypotheses on the mechanisms behind the deep-water thermohaline anomalies. It seems doubtful that the persistent global temperature growth may lead to the opposite decadal trends (positive-then-negative-then-positive, **Fig. 6**) in the deep water salinity.

Our results [Sarafanov et al., 2008; Sarafanov, 2009; Sarafanov et al., 2010b] suggest that natural atmospheric variability over the North Atlantic plays the major role in the deep-water thermohaline variability on a decadal time scale. There are no reasons to associate the deep-water freshening in the 1960s–1990s with climate change, unless the 3-decade-long surface forcing amplification is evidently shown to be a consequence of the latter. Having said that, the net 1950s–2000s trends in the water mass salinities are negative implying that the global factors (e.g., probable intensification of hydrological cycle [Curry et al., 2003]) may act on longer time scales.

1.4.6 Decadal variability of the Deep Western Boundary Current at Cape Farewell

Recent decadal changes in the Deep Western Boundary Current (DWBC) transport southeast of Cape Farewell were assessed from hydrographic data (1991–2007, **Fig. 7a**), direct velocity measurements (2002–2006) and satellite altimetry (1992–2007). Following the approach used in earlier studies [e.g., Bacon, 1998], we first determined that the DWBC (σ_0>27.80) baroclinic transport (T_{BC}) referenced to 1000 m depth increased by ~2 Sv between the mid-1990s (1994–1997) and 2000s (2000–2007) (**Fig. 8b**) [Sarafanov et al., 2009]. In the next step, we quantified velocity changes at the reference level (1000 m) by combining estimates of the hydrography-derived velocity changes in the water column and the altimetry-derived velocity changes at the sea surface [see Sarafanov et al., 2010a]. The inferred increase in the southward

velocity at 1000 m above the DWBC in 1994–2007 indicates that the increase in the DWBC absolute transport was larger but very close to the 2-Sv increase in the DWBC T_{BC}. This result along with the observed coherence of the DWBC absolute and baroclinic transport changes between individual observations [Sarafanov et al., 2010a] imply that the DWBC absolute transport variability in the region is well represented by its baroclinic component on decadal and shorter time scales.

The historical record of the DWBC T_{BC} (1955–2007, **Fig. 8c**) updated after Bacon [1998] shows distinct decadal variability (±2–2.5 Sv) with the transport minima in the 1950s and mid-1990s, maximum in the early 1980s and moderate-to-high transport in the 2000s. The DWBC T_{BC} decadal variability is consistent with the general pattern of the recent decadal hydrographic and circulation changes in the northern North Atlantic. The DWBC T_{BC} anomalies negatively correlate (R = –0.80, 1955–2007) with thickness anomalies of the Labrador Sea Water (LSW) at its origin implying a close link between the DWBC transport southeast of Cape Farewell and the LSW production in the Labrador Sea (**Fig. 8d**). During the recent three decades (late 1970s – late 2000s), the DWBC T_{BC} changes were also in-phase with changes in the strength and zonal extent of the Subpolar Gyre [see Sarafanov et al., 2010a]. In particular, the Gyre weakening at shallow levels in the mid-1990s – mid-2000s was accompanied by the DWBC strengthening in the Irminger Sea [Sarafanov et al., 2009; Sarafanov et al., 2010a; Våge et al., 2011]. The results imply that the decadal changes in the (i) LSW production, (ii) SPG strength and (iii) DWBC transport in the Irminger Sea are linked, representing a complex coherent oceanic response to the decadal variability of the surface forcing.

1.4.7 Mean state of the full-depth circulation in the 2000s

A mean state of the full-depth summer circulation in the Atlantic Ocean in the region in between Cape Farewell (Greenland), Scotland and the Greenland-Scotland Ridge (see **Fig. 3**) was assessed by combining 2002–2008 yearly hydrographic measurements at 59.5°N, mean dynamic topography, satellite altimetry data and available estimates of the Atlantic–Nordic Seas exchange [see Sarafanov et al., 2012]. The mean absolute transports by the upper-ocean, mid-depth and deep currents and the MOC (MOCσ=16.5±2.2 Sv, at σ_0=27.55) at 59.5°N were quantified in the density space. Inter-basin and diapycnal volume fluxes in between the 59.5°N section and the Greenland-Scotland Ridge were then estimated from a box model.

The estimated meridional and diapycnal volume fluxes contributing to the MOC are schematically visualized in **Fig. 9**. The dominant components of the meridional exchange across 59.5°N are the North Atlantic Current (NAC, 15.5±0.8 Sv, σ_0<27.55) east of the Reykjanes Ridge, the northward Irminger Current (IC, 12.0±3.0 Sv) and southward Western Boundary Current (WBC, 32.1±5.9 Sv) in the Irminger Sea and the deep water export from the northern Iceland Basin (3.7±0.8 Sv, σ_0>27.80). About 60% (12.7±1.4 Sv) of waters carried in the MOCσ upper limb (σ_0<27.55) by the NAC/IC across 59.5°N (21.1±1.0 Sv) recirculates westwards south of the Greenland-Scotland Ridge and feeds the WBC. 80% (10.2±1.7 Sv) of the recirculating NAC/IC-derived upper-ocean waters gains density of σ_0>27.55 and contributes to the MOCσ lower limb. Accordingly, the contribution of light-to-dense water conversion south of the Greenland-Scotland Ridge (~10 Sv) to the MOCσ lower limb at 59.5°N is one and a half times larger than the contribution of dense water production in the Nordic Seas (~6 Sv).

1.4.8 Cascading of dense shelf waters in the Irminger Sea

Based on the hydrographic data collected at 59.5°N, 64.3°N and 65–66°N in the western Irminger Sea in the 1990s – 2000s, an observational evidence for the deep-reaching cascading of dense shelf waters south of the Denmark Strait was found [Falina et al., 2012]. The data collected in the northwestern Irminger Sea (65–66°N) indicate that the East Greenland Current ~200 km south of the Denmark Strait occasionally carries shelf waters as dense as the overflow-derived deep waters transported by the DWBC (σ_0 > 27.80). Hydrographic traces of cascading of dense shelf waters down the East Greenland slope were found from repeat measurements at 64.3ºN, where the densest fresh plumes were observed within the DWBC (σ_0 > 27.80) (**Fig. 10**). Using the data collected at 59.5°N, we showed that the fresh 'signals' originating from the shelf can be traced in the DWBC as far downstream as the latitude of Cape Farewell, where the anomalously fresh oxygenated plumes are repeatedly observed in the ISOW and DSOW density classes.

The results of our analysis along with the results from earlier studies [e.g., Rudels et al., 1999; Rudels et al., 2002] indicate that shelf water cascading in the northern Irminger Sea is an intermittent process occurring in all seasons of the year. This implies that, despite the apparent short duration of a particular cascading event, the cumulative contribution of such events to the thermohaline variability and southward export of the deep waters in the WBC can be

considerable. Our tentative estimate based on data from two synoptic surveys at ~59.5°N suggests that the transient contribution of a cascading event in the northern Irminger Sea to the DWBC transport at Cape Farewell can be as large as ~25%.

References

1. Bacon, S. (1998), Decadal variability in the outflow from the Nordic seas to the deep Atlantic Ocean, *Nature*, *394*, 871–874.
2. Boessenkool, K. P., Hall, I. R., Elderfield, H., and I. Yashayaev (2007), North Atlantic climate and deep-ocean flow speed changes during the last 230 years, *Geophys. Res. Lett.*, *34*, L13614, doi:10.1029/2007GL030285.
3. Curry, R., Dickson, R., and I. Yashayaev (2003), A change in the freshwater balance of the Atlantic Ocean over the past four decades, *Nature*, *426*, 826–829.
4. Dickson, R. R., and J. Brown (1994), The production of North Atlantic Deep Water: Sources, rates and pathways, *J. Geophys. Res.*, *99*, C6, 12319–12341.
5. Dickson, R., Yashayaev, I., Meincke, J., Turrell, B., Dye, S., and J. Holfort (2002), Rapid freshening of the deep North Atlantic Ocean over the past four decades, *Nature*, *416*, 832–837.
6. Falina, A., A. Sarafanov, and A. Sokov (2007), Variability and renewal of Labrador Sea Water in the Irminger Basin in 1991–2004, *J. Geophys. Res.*, *112*, C01006, doi: 10.1029/2005JC003348.
7. Falina A., A. Sarafanov, H. Mercier, P. Lherminier, A. Sokov, and N. Daniault (2012), On the cascading of dense shelf waters in the Irminger Sea, *J. Phys. Oceanogr.*, doi:http://dx.doi.org/10.1175/JPO-D-12-012.1.
8. Gladyshev S., V. Gladyshev, A. Falina, A. Sarafanov (2016), Winter convection in the Irminger Sea in 2004-2014, *Oceanology,* doi*:* 10.1134/S0001437016030073.
9. Gladyshev S., V. Gladyshev, S. Gulev, A. Sokov (2016), Anomalously deep convection in the Irminger Sea during the winter of 2014–2015, *Doklady Earth Sciences* doi: 10.1134/S1028334X16070229.
10. Gladyshev S., V. Gladyshev, L. Pautova, S. Gulev, A. Sokov (2018), Intermediate waters in the Irminger Sea during deep convection: variability and the role of circulation mechanisms, *Doklady Earth Sciences*, doi: 10.1134/S1028334X18120127.
11. Hansen, B., Osterhus S., Quadfasel D., and W. Turrell (2004), Already the day after tomorrow?, *Science*, *305*, 953–954.
12. Hurrell, J. W. (1995), Decadal trends in the North Atlantic Oscillation: regional temperatures and precipitation, *Science*, *269*, 676–679.

13. Koltermann, K. P., A. Sokov, V. Tereschenkov, S. Dobroliubov, K. Lorbacher, and A. Sy (1999), Decadal changes in the thermohaline circulation of the North Atlantic, *Deep Sea Res.*, *Part II*, *46*, 109–138, doi:10.1016/S0967-0645(98)00115-5.
14. Lherminier, P., H. Mercier, T. Huck, C. Gourcuff, F. F. Perez, P. Morin, A. Sarafanov, and A. Falina (2010), The Atlantic Meridional Overturning Circulation and the subpolar gyre observed at the A25–Ovide section in June 2002 and 2004, *Deep-Sea Res.*, *Part I*, *57*, 1374–1391, doi:10.1016/ j.dsr.2010.07.009.
15. Meehl, G. A., (2007), Global climate projections. Climate Change 2007: The Physical Science Basis, S. Solomon et al., Eds., Cambridge University Press, 747–847.
16. Pickart, R. S., Spall, M., Ribergaard, M. H., Moore, G. W. K. and R. Milliff (2003), Deep convection in the Irminger Sea forced by the Greenland tip jet, *Nature*, *424*, 152–156.
17. Rudels B., Eriksson P., Grönvall H., Hietala R. and Launiainen J. (1999), Hydrographic Observations in Denmark Strait in Fall 1997, and their Implications for the Entrainment into the Overflow Plume, *Geophys. Res. Lett.*, *26*, 1325–1328.
18. Rudels, B., E. Fahrbach, J. Meincke, G. Budeus, and P. Eriksson (2002), The East Greeenland Current and its contribution to the Denmark Strait overflow, *ICES J. Marine Science*, *59*, 1133–1154.
19. Sarafanov, A., A. Sokov, A. Demidov, and A. Falina (2007), Warming and salinification of intermediate and deep waters in the Irminger Sea and Iceland Basin in 1997–2006, *Geophys. Res. Lett.*, *34*, L23609, doi:10.1029/2007GL031074.
20. Sarafanov, A., A. Falina, A. Sokov, and A. Demidov (2008), Intense warming and salinification of intermediate waters of southern origin in the eastern subpolar North Atlantic in the 1990s to mid-2000s, *J. Geophys. Res.*, *113*, C12022, doi:10.1029/2008JC004975.
21. Sarafanov, A. (2009), On the effect of the North Atlantic Oscillation on temperature and salinity of the subpolar North Atlantic intermediate and deep waters, *ICES J. Marine Science*, *66 (7),* 1448–1454, doi:10.1093/icesjms/fsp094.
22. Sarafanov, A., A. Falina, H. Mercier, P. Lherminier, and A. Sokov (2009), Recent changes in the Greenland–Scotland overflow-derived water transport inferred from hydrographic observations in the southern Irminger Sea, *Geophys. Res. Lett.*, *36*, L13606, doi:10.1029/2009GL038385.

23. Sarafanov A., A. Falina, P. Lherminier, H. Mercier, A. Sokov, and C. Gourcuff (2010a), Assessing decadal changes in the Deep Western Boundary Current absolute transport southeast of Cape Farewell (Greenland) from hydrography and altimetry, *J. Geophys. Res.*, *115*, C11003, doi:10.1029/2009JC005811.

24. Sarafanov A., H. Mercier, A. Falina, A. Sokov, and P. Lherminier (2010b), Cessation and partial reversal of deep water freshening in the northern North Atlantic: observation-based estimates and attribution, *Tellus*, *62A*, 80–90, doi:10.1111/j.1600-0870.2009.00418.x.

25. Sarafanov A., A. Falina, H. Mercier, A. Sokov, P. Lherminier, C. Gourcuff, S. Gladyshev, F. Gaillard, and N. Daniault (2012) Mean full-depth summer circulation and transports at the northern periphery of the Atlantic Ocean in the 2000s, *J. Geophys. Res.*, *117*, C01014, doi:10.1029/2011JC007572.

26. Schmitz, W. J., Jr., and M. S. McCartney (1993), On the North Atlantic Circulation, *Rev. Geophys.*, *31*, 29–49.

27. Schott, F. A., and P. Brandt (2007), Circulation and deep water export of the subpolar North Atlantic during the 1990s, *in Ocean Circulation: Mechanisms and Impacts*, *Geophys. Monograph Series*, *173*, Eds. A. Schmittner, J. Chiang, and S. Hemmings, 91–118, doi:10.1029/173GM08.

28. Sutherland, D. A., and R. S. Pickart (2008), The East Greenland Coastal Current: structure, variability, and forcing, *Prog. Oceanogr.*, *78*, 58–77, doi:10.1016/j.pocean.2007.09.006.

29. Våge K., R. Pickart, A. Sarafanov, Ø. Knutsen, H. Mercier, P. Lherminier, H. van Aken, J. Meincke, D. Quadfasel, and S. Bacon (2011a), The Irminger Gyre: circulation, convection, and interannual variability, *Deep-Sea Res. Part I*, *58*, 590–614, doi:10.1016/j.dsr.2011.03.001.

30. van Aken, H. M. (2007), The oceanic thermohaline circulation: An introduction, New York, Springer, 326 p., ISBN 978-0-387-36637-1.

31. Yashayaev, I. (2007), Hydrographic changes in the Labrador Sea, 1960–2005, *Prog. Oceanogr.*, *73*, 242–276.

.

1.5 Preliminary Results

The upper-ocean, mid-depth and deep water circulation patterns, merging the results of the present analysis with those from the earlier studies [e.g., *Macrander et al.*, 2005; *Østerhus et al.*, 2005, 2008; *Schott and Brandt*, 2007; *Sutherland and Pickart*, 2008; *Lherminier et al.*, 2010; *Våge et al.*, 2011], are schematically visualized Figures 12–14. A schematic diagram of the meridional overturning circulation in the Atlantic Ocean north of 59.5°N is displayed in **Fig. 9**.

The results provide the following conceptual view of the gyre / overturning circulation at the northern periphery of the Atlantic Ocean in the 2000s.

The NAC and IC collectively carry 21.1 ± 1.0 Sv of warm upper-ocean waters across 59.5°N northwards within the MOCσ upper limb ($\sigma_0 < 27.55$). About 40% of this flow forms the Atlantic Inflow to the Nordic Seas, and 60% (12.7 ± 1.4 Sv) recirculates westwards in the subpolar gyre northern limb south of Iceland to feed the WBC in the Irminger Sea. Only 20% (2.4 ± 1.2 Sv) of the recirculating NAC/IC-derived waters exits the Irminger Sea in the WBC at shallow levels ($\sigma_0 < 27.55$), while 80% (10.2 ± 1.7 Sv, a half of the NAC/IC northward flow across 59.5°N) gains density of $\sigma_0 > 27.55$ and enters the MOCσ lower limb. The resulting net southward transport in the MOCσ lower limb at the latitude of Cape Farewell is 16.5 ± 2.2 Sv, of which ~60% (~10.2 Sv) is due to light-to-dense water transformation south of the GSR.

As no dense-to-light water re-conversion is expected to occur in the subpolar gyre, the NAC/IC-derived waters, once entering the MOCσ lower limb in the Irminger Sea, will eventually contribute to the MOCz lower limb (~11 Sv at 59.5°N) at the southern margin of the subpolar region. There, at ~48°N, the MOCσ and MOCz are of nearly the same magnitude, 16 ± 2 Sv, as estimated from data collected in the 1990s [see *Schott and Brandt*, 2007; *Lumpkin et al.*, 2008]. This is very close to our estimate of the mean MOCσ at 59.5°N. The comparison is tentative, though, because it does take into account the decadal variability of the MOC [*Koltermann et al.*, 1999; *Willis*, 2010]. With this caveat in mind, our results imply a minor contribution to the MOCσ by the net dense water formation in the subpolar gyre between ~48°N and 59.5°N. This inference concurs with the results by *Pickart and Spall* [2007] suggesting a

minor contribution to the Atlantic MOC by the net water mass transformation in the Labrador Sea.

To conclude, the results of the present study, verified with independent estimates where possible, provide the first observation-based quantitative view of a mean state of the gyre / overturning circulation at the northern periphery of the Atlantic Ocean. The most interesting features of the obtain circulation pattern are as follows:

• Nearly half of volume of the upper-ocean waters transported northward across 59.5°N in the eastern limb of the subpolar gyre (NAC and IC, $\sigma_0 < 27.55$) overturns in the density plane south of the GSR and feeds the lower limb of the Atlantic MOCσ.

• The contribution to the MOCσ lower limb at 59.5°N by overturning (light-to-dense transformation) of the NAC / IC-derived upper-ocean waters south of the GSR is one and a half times as large as the contribution of the Nordic Seas overflows.

• The net southward flow in MOCσ lower limb at 59.5°N is associated primarily with the deep water ($\sigma_0 > 27.80$) export. Nearly half of the net southward flow of deep waters across 59.5°N is due to entrainment of the Atlantic waters in the Irminger Sea.

• The DWBC at 59.5°N is fed primarily by the Denmark Strait Overflow and by the diapycnal flux / entrainment from the mid-depth layer, while the contribution to the DWBC transport from the ISOW flow is minor. A major part of the ISOW transported into the Irminger Sea from the Charlie-Gibbs Fracture Zone recirculates southward in the eastern Irminger Sea and exits the basin via an interior pathway rather than along the western boundary. The results can be used for validation of numerical models. From this perspective, multi-year mean transports have an obvious advantage over individual section-based synoptic estimates, which bear the impress of vigorous variability occurring on a variety of spatial and temporal scales. The methodological outcome is that the combined use of repeat hydrography, the MDT by *Rio and Hernandez* [2004] and satellite altimetry data can provide a useful estimate of the mean full-depth circulation across a transatlantic section without imposing *a priori* constraints.

1.6 Major Problems and Goals Not Achieved

OS75 kHz VM ADCP was out of range after finalizing the Denmark Strait section. MRU 3 was rebooted a few times that took 10-20 minutes.

2. CONTINUOUS MEASUREMENTS (on station and underway)

2.1 Navigation

Navigation data from Trimble SPS 461 GPS was recorded every 1 second and was stored on the PC in binary format.

2.2 Meteorological Measurements

The standard mean meteorological measurements were stored in the separate files on the same PC with navigation data. Recording were running about 1 day later after departure from Kaliningrad (Russia) on 8th August, and worked reliably until completion of the cruise in Kaliningrad (Russia) on 12th September. Variability of the atmospheric pressure, air temperature and wind speed and direction from August 9th are shown in **Fig. 11-13**.

2.3 Echosounding

The bathymetric equipment aboard during RV Akademik Sergey Vavilov Cruise 50 consists of EA600 12 kHz hydrographic echosounder. Data were collected for most of the cruise. The Hull mounted transducer is located 5.8 metres below the sea surface and this value was entered to estimate the depth.

Depth was indicated on the echosounder display and stored on the separate PC together with the navigation.

2.4 Vessel Mounted Acoustic Doppler Current Profiler (VMADCP) OS 75 kHz

The Ocean Surveyor 75 kHz is designed for vessel-mount current profile measurement in the upper ocean water from depths greater than 30-50 meters. The system consists of a transducer and electronics chassis connected to PC. Data are transmitted in binary format through the I/O cable. GPS data in NMEA format are transmitted separately to another PC COM – port. The VMADCP can operate in two regimes (Narrow Bandwith and Broad Bandwith Profiling). Its main specifications are shown below. To increase the collected data accuracy we used the Broad Band mode.

To collect OS 75 kHz data we used *VmDas* software (version 1.48). The NMEA messages *VmDas* reads are standard GGA, HDG, HDT, VTG messages.

	Bin size	Maximum range	Accuracy (cm/s)
Narrow Band (long-range mode)	16 m	560 - 700 m	16
Broad Band (high-precision mode)	16 m	350 - 450 m	7

We used a following configurations to collect the data.

WP00001 – Broad Bandwidth profiling
WN045 – number of bins 45
WF1600 – blanking size 16 m
BP00 – no bottom track (BP),
BP01 – bottom track (BP) for the sea depth less than 1000 m, and
BP00 – for the deep basins

VmDas saves data in a few files with extension ENX, ENS, ENR (raw data with and without navigation), NR – NMEA messages, STA and LTA averaged data. Misalignment angle was introduced in configuration file and was used by VmDas for data correction. We calculated the misalignment angle for each section with bottom track data.

Data processing performed STA files with 40-profile averaging. Taking into account that single ping takes about 3 seconds, one 40-profile ensemble lasts near 120 seconds in Broad Bandwidth regime.

Data processing consists of data conversion in NetCDF format with extension NC and further cleaning, tide removing (using barotropic tidal model TPXO 7.2) and averaging. IFREMER software was used to process OS 75 kHz data.

3. ON-STATION MEASUREMENTS

3.1 CTD

3.1.1 Equipment

The deep profiler system used during the cruise included the following components: SBE 32 painted aluminum 24 bottle multisampler frame, SBE 9P-727 CTD, Up (WHS -300 kHz) and Down looking (WHS -300 kHz) RD Instruments Acoustic Doppler Current Profiler (LADCP), Separate Battery pack pressure case ext. 6000 m connected to LADCPs with star cable, 22 x 5 liter Test Oceanic Niskin bottles, Benthos altimeter PSA-916.

Lab equipment for data acquisition and archiving of CTD/LADCP data consisted of the following items mounted on the deck. Mini PC Shuttle XH310V/Intel Core i5-8400/16Гб Ram/240Гб SSD, APC Back-UPS 550VA/330W, SBE 11p Deck Unit.

Cruise Preparation

Equipment and sensors were assembled when the ship crossed the Baltic and North Seas (08-09th June). Water bottles were checked for integrity of seals, taps, stoppers and lanyards before being fitted and roped to the multisampler frame.

Deployment

The CTD was deployed with a lowering rate of 60 meters/min (30-40 meters/min in the upper 200 meters or deeper if the conditions are rough). It is recovered at a rate of 60 meters/min.

The LADCPs fitted within the frame with a separate battery pressure case performed well. These units contain a compass and tilt sensors which could possibly provide useful information on the attitude and rotation of the whole profiler package throughout deployments.

Bottle firing using the deck unit and pylon was very reliable during the cruise.

Operationally this has been a successful cruise with virtually no time being lost due to mechanical or equipment failure.

3.1.2 Data processing and calibration

CTD data were logged at 24 scans per second and passed from the CTD deck unit to the PC.

The CTD data was recorded onto disk by the PC using SEABIRD SEASOFT-Win 32: Seasave V7, Software Release 7.26.7. A screen display of temperature, oxygen, salinity and density profiles vs pressure are used to decide the depths at which bottles are to be tripped on the up cast. The bottles are tripped using the enable and fire buttons on the PC screen. During post-processing, the SEASAVE software stores 35 scans at each bottle trip within a separate file. At the end of the station, all the data and header files associated with the station are transferred immediately via ethernet to the second PC. The SBE data processing software is used to create 1 dbar processed data files.

The data processing takes the following steps:

DATCNV Converts the raw data to physical parameters.

WILDEDIT For every block of 100 scans, flags all scans whose pressure, temperature, conductivity and oxygen values differ from the mean by more than 2 standard deviations. Recomputes mean from unflagged data then marks as bad all scans exceeding 20 standard deviations from these new values.

FILTER Low pass filter pressure channel with time constant used for pressure 0.150 seconds.

ALIGNCTD Aligns the oxygen values relative to the pressure values accounting for the time delays in the system. Time offsets of 4.000 secs for oxygen are used.

CELLTM A recursive filter used to remove the thermal mass effects from the conductivity data. Thermal anomaly amplitude and time constants of 0.0300 and 7.0000 were used.

LOOPEDIT Marks as bad, all cycles on the down trace for which the vertical velocity of the CTD unit is less than 0.25 metres/sec.

WINDOW FILTER cosine filter temperature and conductivity, window size 23 scans.

DERIVE Computes salinity, potential temperature, sigma-t, sigma theta and oxygen values.

BINAVG Averages the down cast into 1 dbar pressure bins.

SPLIT Splits the data into DOWN and UP cast.

Calibration data

The CTD calibrations used during this cruise were supplied by Sea Bird Electronics and are as follows:

Pre-cruise calibration:

CALIBRATION DATE: 12-Aug 2016 (all stations)

Conductivity Sensor S/N 044580

G=-9.90055574e+000

H=1.24515002e+000

I=-1.59442188e-005

J=5.25554824e-005

CPcor=-9.57000000e-008
CTcor=3.2500e-006

Pre-cruise calibration:
CALIBRATION DATE: 09-Aug-16 (all stations)
Temperature Sensor S/N 036082
Temperature ITS-90 = 1/{g + h[*ln*(f0/f)] + i[*ln*2(f0/f)] + j[*ln*3(f0/f)]} - 273.15 (°C)
Following the recommendation of JPOTS: T68 is assumed to be 1.00024 * T90 (-2 to 35°C)
f is the frequency
G=4.33833475e-003
H=6.37459433e-004
I=2.21244493e-005
J=2.06389145e-006
F0=1000.000

Pressure Sensor S/N 93694 **(all stations) no drift**
CALIBRATION DATE: 28-Feb-16
C1 = -4.206220e+004
C2 = -1.248757e+000
C3 = 1.284830e-002
D1 = 3.551700e-002
D2 = 0.000000 e+000
T1 = 3.003496e+001
T2 = -5.977825e-004
T3 = 3.851680e-006
T4 = 1.762330e-009
T5 = 0.000000 e+000
AD590M = 1.287870e-002
AD590B = -8.515870e+000
Slope = 1.00000
Offset = 0.0 (dbars)

Oxygen Sensor 430699
CALIBRATION DATE: 23-Jul-2017 (All Stations)

Soc = 4.5067e-001
Voffset = -0.5492
Tau20 = 1.16000e+000
A = -2.87830e-003
B = 1.46410e-004
C = -2.74880e-006
E nominal = 3.60000e-002
D1 = 1.92634e-004
D2 = -4.64803e-002
H1 = -3.30000e-002
H2 = 5.00000e+003
H3 = 1.45000e+003

3.1.3 Final Post-Cruise CTD Calibrations

Temperature Calibration Temperature Sensor 036082

0.0000 sensor drift was applied to the temperature data based on the *pre cruise calibration coefficients* for all stations.

Pressure Calibration Pressure Sensor S/N 93694

Final CTD pressure correction: Since no drift for pressure sensor was defined by SeaBird Electronics pressure was corrected for atmospheric pressure only. With offset in *.con* or *.xmlcon* file set to -0.0026 db, pressure measured by CTD should equal barometric pressure

• Calculate offset (db) = barometer reading – CTD reading

– Conversion of psia to decibars: decibars = (psia - 14.7) * 0.6894759

• Enter calculated offset in *.con* or *.xmlcon* file

• Example:

– CTD reads -2.5 dbars

– Barometer reads 14.65 psia.

Converting to decibars, barometer reads (14.65 - 14.7) * 0.6894759 = -0.034 dbars

– offset (db) = barometer reading – CTD reading = -0.034 - (-2.5) = 2.466

Salinity Calibration Conductivity Sensor 044580

We used *pre-cruise calibration coefficients* with slope correction according to App. Notes No 31 (Revised February 2010).

If **α** is the conductivity computed from the **pre-cruise bath data** (temperature and frequency) using **post-cruise calibration coefficients** and **β** is the true conductivity in the **pre-cruise bath**, then:

$$\textbf{postslope} = \frac{\sum_{i=1}^{n} (\alpha_i)(\beta_i)}{\sum_{i=1}^{n} (\alpha_i)(\alpha_i)} \qquad \text{(postslope is typically < 1.0)}$$

Sea-Bird calculates and prints the value for postslope on the conductivity calibration sheet for all calibrations since February 1995 (see *Appendix I: Example Conductivity Calibration Sheet*)

To correct conductivity data taken between pre- and post-cruise calibrations:

islope = 1.0 + (b / n) [(1 / postslope) - 1.0]

where

islope = interpolated slope; this is the value to enter in the configuration (.con or .xmlcon) file
b = number of days between pre-cruise calibration and the cast to be corrected
n = number of days between pre- and post-cruise calibrations
postslope = slope from calibration sheet as calculated above (see *Appendix I: Example Conductivity Calibration Sheet*)

In the configuration (.con or .xmlcon) file, use the **pre-cruise calibration coefficients** and use **islope** for the value of slope.*

Note: In our SEASOFT V2 suite of programs, edit the CTD configuration (.con or .xmlcon) file using the Configure Inputs menu in Seasave V7 (real-time data acquisition software) or the Configure menu in SBE Data Processing (data processing software).

For typical conductivity drift rates (equivalent to -0.003 PSU/month), islope does not need to be recalculated more frequently than at weekly intervals.

3.1.4 SBE 43 Dissolved Oxygen Sensor Calibration using Winkler Titrations

We use a method for statistically estimating calibration coefficients for calculating dissolved oxygen in milliliters per liter from SBE 43 output voltage. The technique requires dissolved oxygen concentration in ml/l (determined from Winkler titration of water samples) and SBE 43 oxygen voltage outputs at the times the water samples were collected. Sea-Bird's data processing software, SBE Data Processing, is used to produce a data table suitable for the analysis.

Background

The equation used in Sea-Bird's software for calculating dissolved oxygen in ml/l from SBE 43 output voltage is a form of that given in Owens-Millard (1985):

$$Oxygen\ (ml/l) = \left\{ Soc * \left(V + Voffset + tau(T,P) * \frac{\partial V}{\partial t} \right) \right\} * Oxsol(T,S) * \left(1.0 + A*T + B*T^2 + C*T^3\right) * e^{\left(\frac{E*P}{K}\right)} \qquad eqn\ 1$$

where:

- V = SBE 43 output voltage signal (volts)
- $\partial V/\partial t$ = time derivative of SBE 43 output signal (volts/second), computed over a default window of 2 seconds
- T = CTD temperature (°C)
- S = CTD salinity (psu)
- P = CTD pressure (dbars)
- K = CTD temperature (°K = °C + 273.15)
- *tau(T,P)* = sensor time constant at temperature and pressure
- *Oxsol(T,S)* = oxygen solubility function (ml/L), which converts oxygen partial pressure (sensor measurement) to oxygen concentration (*Garcia and Gordon, 1992*). See Appendix A in *Application Note 64: Background Information, Deployment Recommendations, and Cleaning and Storage* for values at various temperatures and salinities.
- *Soc, Voffset, A, B, C, E*, and *tau20, D1, D2* [terms in calculation of *tau (T,P)*] are calibration coefficients

The SBE 43 is expected to provide an output voltage that is linear with respect to oxygen concentration. Normal calibration drift manifests itself as a loss of sensitivity and is evident as a change of slope (and less so in offset) in the linear relationship between oxygen concentration and voltage output. The coefficients *A, B, C,* and *E* correct for small secondary responses to temperature and pressure. Because these coefficients change very slowly over time, the values given on the SBE 43 calibration certificate will be used in this analysis, and we will concern ourselves with estimating changes in the slope (Soc) and offset (Voffset).

Setting $\frac{\partial V}{\partial t}$ to zero, we rearrange equation 1 into a linear form and perform a linear regression to obtain a new *Soc* and *Voffset*.

Let:

$$\phi = Oxsol(T,S) * \left(1.0 + A*T + B*T^2 + C*T^3\right) * e^{\left(\frac{E*P}{K}\right)} \qquad eqn\ 2$$

The oxygen equation then reduces to the form in equation 3:

$$Oxygen(ml/l) = Soc * (V + Voffset) * \phi \qquad eqn\ 3$$

This may be expressed in a linear form in equation 4.

$$\frac{Oxygen(ml/l)}{\phi} = Soc * (V + Voffset) = M * V + B \qquad eqn\ 4$$

Where:

Soc = M
Voffset = B / M

A linear regression is calculated using Winkler oxygen concentration divided by ϕ as the dependent variable and SBE 43 output voltage as the independent variable.

Winkler oxygen divided by φ versus SBE 43 output voltage for this cruise is shown in

Fig. 14 and include linear regression lines calculated from the data.

The final coefficients are for transatlantic section (sta 2756 – 2832)
Soc=4.2728e-001
Voffset=-0.4158
1359 oxygen samples were used to build this linear fit for sill sections.

The final coefficients are for the Reykjanes section (sta 2833 – 2866)
Soc=4.3503e-001
Voffset=-0.4557
513 oxygen samples were used to build this linear fit for sill sections

The final coefficients are for the DS section (sta 2867 – 2901)
Soc=4.4193e-001
Voffset=-0.5015<
294 oxygen samples were used to build this linear fit for sill sections

The final coefficients are for the IFS sections (sta 2902 – 2951)
Soc=4.4379e-001
Voffset>-0.4900
630 oxygen samples were used to build this linear fit for sill sections.

Procedure

The linear regression that yields a new *Soc* and *Voffset* may be accomplished with spreadsheet software, a hand-held calculator with statistical capability, or (with perseverance) a calculator, graph paper, and pencil. As a first step, extract pressure, temperature, salinity, oxygen saturation, and SBE 43 voltage from the parts of your CTD data collected when the water sampler closures occurred.

Run SBE Data Processing, and select Data Conversion in the Run menu. Select the appropriate configuration (*.con*) and data (*.dat* or *.hex*) files on the *File Setup* tab. Click the *Data Setup* tab and set *Convert data from* to *Upcast and downcast* and *Create file types* to *Create bottle (.ros) file only*.

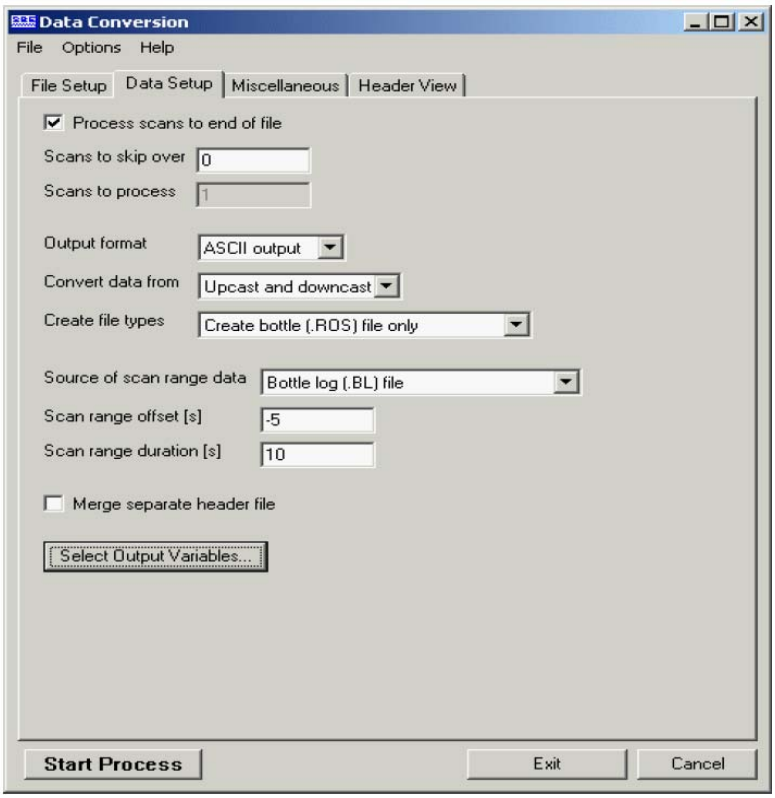

To extract CTD data concurrent to the water sampler closures, Data Conversion must know when the closures occurred. Select an appropriate *Source of scan range data*, depending on your instrument type and how the sampler was commanded to close bottles:

- SBE 9*plus* with SBE 11*plus* or 17*plus* - The data stream is marked with a *bottle confirm* bit each time a closure occurred.
- Using SEASAVE to operate the water sampler - A *.bl* file, with scan ranges corresponding to closures, is created during the cast.
- SBE 19, 19*plus*, 19*plus* V2, or 25 with Auto Fire Module (AFM) and SBE 32 Carousel Water Sampler, or operated autonomously with SBE 55 ECO Water Sampler - The *.afm* file contains scan ranges.

Like all sensors, the SBE 43 has a finite response time to a change in dissolved oxygen concentration. This response time is usually on the order of 6 seconds. For this reason, good sampling procedure dictates that the instrument package should be stopped in the water column long enough for the SBE 43 and all other sensors to completely equilibrate before closing the water sampler. An equilibration time of 5 to 6 response times, or 30 to 36 seconds, is adequate.

In the example above, Data Conversion will begin extracting data 5 seconds before each water sampler closure (*Scan range offset = -5 s*) and will extract a total of 10 seconds of data (*Scan range duration = 10 s*). Note that 10 seconds is longer than the SBE 43 response time. Because we are extracting data for 5 seconds after the water sampler closure, the instrument package must remain stopped for at least this long.

To estimate *Soc* and *Voffset*, you need pressure, temperature, salinity, oxygen saturation (ml/l), and SBE 43 Oxygen Voltage to go with each Winkler titration data value. Click *Select Output Variables* and add each of the required parameters; the dialog box is shown below.

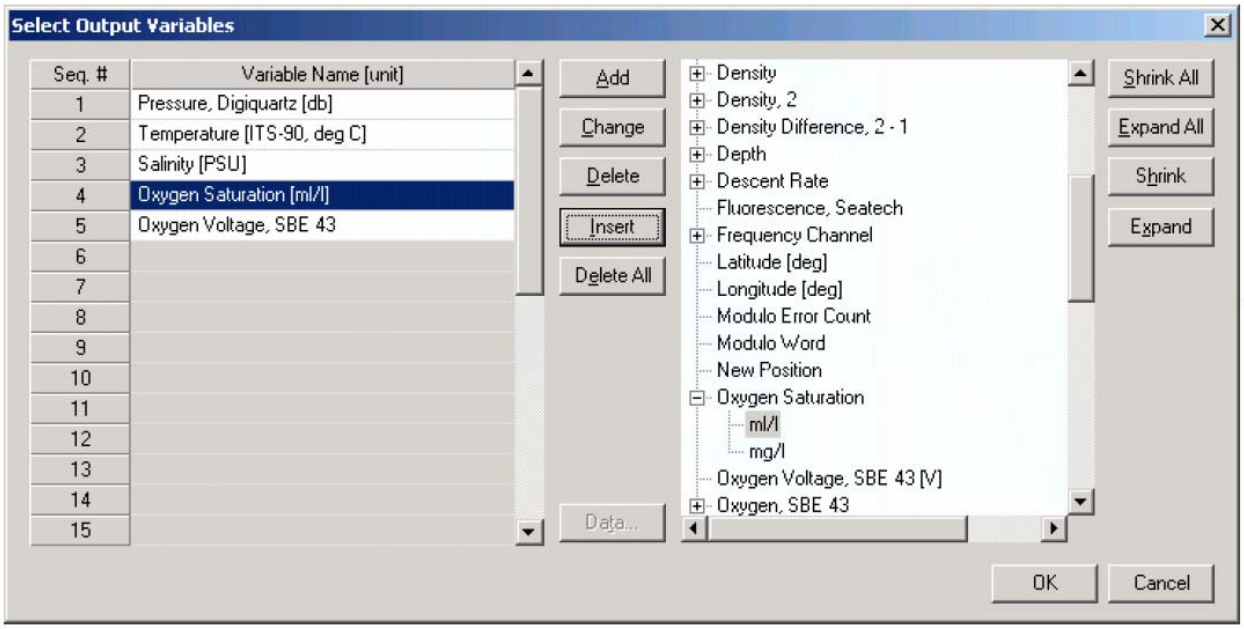

After selecting all the variables, click *OK* to return to the Data Conversion Data Setup tab. Then click *Start Process* to create the *.ros* file.

For this example, the *.ros* file contains 10 seconds of data centered on the moment the bottle closure occurred for every bottle closure. To make a useful table, select Rosette Summary from SBE Data Processing's Run menu. Rosette Summary calculates averages and standard deviations for the variables selected in Data Conversion. Select the appropriate *.con* and *.ros* files on the *File Setup* tab. Click the *Data Setup* tab and then click the *Select Averaged Variables* button; the dialog box is shown below.

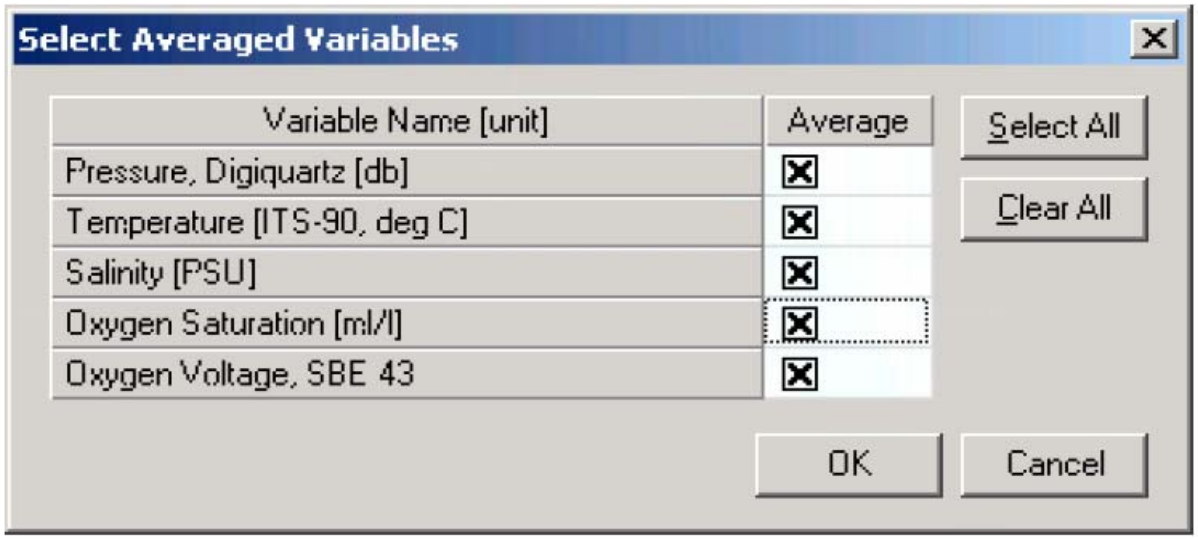

After selecting all the variables, click *OK* to return to the Rosette Summary Data Setup tab. Then click *Start Process* to create a data table file with the *.btl* extension.

Create a table with average pressure, temperature, salinity, oxygen saturation, and SBE 43 output voltage for each water sampler closure depth, by importing the *.btl* file into a spreadsheet. Then, enter by hand the Winkler titration dissolved oxygen values from your titration log, matching water sampler closures to pressures.

Calculate $\phi = Oxsol(T,S) * \left(1.0 + A*T + B*T^2 + C*T^3\right) * e^{\left(\frac{E*P}{K}\right)}$,

using *A, B, C,* and *E* from the SBE 43 calibration sheet.
Then, calculate $Winkler\ O_2 / \phi$.

Perform a linear regression, with:

- $Winkler\ O_2 / \phi$ (shown as Winkler/phi in the table) as the *Y* data
- SBE 43 output voltages as the *X* data

If a spreadsheet or statistical calculator is not available, the regression equations are:

$$M = \frac{n * \sum\left(V * \frac{Winkler\ O_2}{\phi}\right) - \sum V * \sum\left(\frac{Winkler\ O_2}{\phi}\right)}{n * \sum V^2 - \left(\sum V\right)^2}$$

$$B = \frac{\sum\left(\frac{Winkler\ O_2}{\phi}\right) - M * \sum V}{n}$$

Where:

n = number of data pairs
M = Slope
B = Offset

And:

$Soc = M$
$Voffset = B/M$

Reference

Owens, W. B., and R. C. Millard Jr., 1985: A new algorithm for CTD oxygen calibration. J. Phys. Oceanogr., 15, 621-631.
(NOTE: calibration expressed as ml/l)

3.2 Oxygen Bottle Samples

Oxygen samples were drawn first from every bottle. Duplicate samples were taken on each cast, usually from the first two bottles. Samples were drawn into clear, wide necked calibrated glass bottles and fixed on deck with reagents dispensed using Aquastep bottle top dispensers. A test station used to check on the oxygen bottle calibrations and as an opportunity to train a number of people to take the samples. The samples were shaken on deck and again in the laboratory 1/2 hour after collection, when the bottles were checked for the tightness of the stoppers and presence of bubbles. The samples were then stored under water until analysis.

Bottle temperatures were taken, following sampling for oxygen, using a hand held electronic thermometer probe. The temperatures were used to calculate any temperature-dependent changes in the sample bottle volumes.

Samples were analyzed in the constant temperature laboratory, starting three hours after sample collection, following the Winkler whole bottle titration with an amperometric method of endpoint detection, as described by Culberson (1991). The equipment used was supplied by Metrohm and included the Titrino unit and control pad, exchange unit with 10 ml burette to dispense the thiosulphate in increments of 2 µl , with an electrode for amperometric end point detection.
The difference for the duplicate pairs sampled on each station was in a range **0.00-0.02** ml/l .

The thiosulphate normality was checked on each run and recalculated every time the reservoir was topped up against potassium iodate. The exact weight of this standard, the calibrated 5 ml exchange unit driven by a Metrohm Dosimat and the 1L glass volumetric flask used to dispense and prepare the standard.

The introduction of oxygen with the reagents and impurities in the manganese chloride were corrected for by blank measurements made on each run, as described in the WOCE Manual of Operations and Methods (Culberson, 1991).

Collected data shows that dissolved oxygen concentrations varied from **4.85** to **8.71** ml/l. In order to control the accuracy of the oxygen measurements at each cast were taken parallel samples from the 1-2 bottles or duplicate samples.

Reproducibility of measurements

2898 samples were taken during the cruise; in addition **93** duplicates were analyzed. These include both duplicates taken from the same bottle (replicates) and those taken from different bottles fired at the same depth. The data gave a standard deviation of **0.008** ml/l.

References:

Culberson, C.H. 1991.15 pp in the WOCE Operations Manual (WHP Operations and Methods) WHPO 91/1, Woods Hole.

Modern methods of hydrochemical research of the ocean, 1992. IO RAS, Moscow (in Russian).

3.3 Lowered Acoustic Doppler Current Profiler (LADCP)

The TRDI WHS 300 kHz ADCPs consists of a pressure case rated to 6000 meters with 4 transducers at one end in a convex arrangement and the beams diverging at 20 degrees from the vertical. At the opposite end to the transducers is a connector that enables downloading of data and connects it to other pressure cases containing another ADCP and the power supply pack. This arrangement allowed the ADCPs and the battery pack to be mounted vertically as up and down-looking on the CTD frame. Connection amongst all units was established using star cable with three male and two female terminations. Two male cable ends were always attached to the frame, this enabled comms leads to be readily connected pre and post deployment.

Communications: The 20-m communication leads (which also allow external power to be supplied to the ADCP) were sufficiently long to route it through to the port side of the deck lab where it was connected to a dedicated PC and external power supply. The latter was set at 48+ volts and was left on whilst the ADCP was on deck. 5 minutes prior to deployment the external power supply was shut off, the instrument checked and the configuration file sent to the ADCP as described in the manual instructions. The free end of the fly leads was greased and the end cap refitted, this was then taped to the frame for security.

Post deployment: When the CTD/LADCP was brought inboard, the fly-lead connectors were dried and the comms leads were connected to them. This stopped undue bending of the cables and kept them clear of the water bottles, aiding sampling. External power was applied again and the cast data downloaded as per the manual with a baud rate of 57600. The processing is accomplished using software developed by Visbeck after transferring the data to the PC.

Battery power was supplied to the ADCP in the form of 42 volts from 28 x 1.5 volt alkaline cells. Four of these packs were available for the cruise, as the ADCP will function at a minimum of 32 volts this was deemed an adequate stock for the duration.

Data quality: The data quality from the ADCP was good throughout. Due to the bad weather instrument titles sometimes exceeded 12° and this data was rejected during processing.

The LADCPs seem to function well and generates useful information on currents. The battery supply has its limitations though and thought should be given to alternatives to the present set-up.

3.3.1 LADCP Processing for Current Profiles

A brief account of the LADCP current data processing, file nomenclature and directory structure is provided in the following lines. Little emphasis is put into a detailed description of the main programming tools used, since these are part of a standard software package developed by Gerd Krahmann (**version 10.13**).

Outline of LADCP current calculation method

The Broad Band LADCP used during ASV50 cruise was designed to measure the instantaneous relative velocities of scatterers in the water column by taking advantage of the Doppler frequency shift, phase changes and correlation between coded pulses transmitted and received by the LADCP's four transducers. Conversion of this raw data stream to a profile of absolute currents involved an elaborate calculation method.

Firstly, Doppler shifts needed to be scaled to velocity units by taking into account the depth-dependent sound velocity (estimated from CTD T and S measurements). Directions could be inferred from trigonometric calculations based on the geometry of the transducer set, the orientation of the package (measured with a flux gate compass) and the local magnetic declination. The depth of the instrument was calculated from the integration of the measured vertical velocity and later adjusted to match the depth given by the CTD's pressure sensor.

The velocities corresponding to each single ensemble (or, in effect, to each transducer ping) were gridded in bins of depth set 10 meters. Statistical rejection of spiky measurements within each of these bins followed.

In order to reject the unwanted motion of the instrument (but also the barotropic component of the current), shear profiles were calculated for each ensemble. A complicated editing scheme preceded this shear calculation. A final shear profile (baroclinic current) was derived by real- depth gridding of the shear profiles calculated for individual ensembles. It was hoped that any relative velocities introduced by the high-frequency motion of the CTD package would be smoothed out by this repeated averaging.

The barotropic component of the flow was finally calculated from bottom-tracking measurements (bottom-track mode) or, in most occasions, in an integral sense from differential GPS positions of the ship (water-track mode).

The definitive velocity profile was hence obtained as the sum of the baroclinic and barotropic components.

During ASV50 cruise, no specific error calculation was performed. Profiles of shear standard deviation were included in the cast log sheet folder. Internal wave signals were obvious throughout the cruise.

Relevant PC files

The raw data were downloaded from the LADCP into a devoted PC after each cast and stored as a binary file called vNNNNm_01.000 for Master and vNNNNs_01.000 for Slave the c:\ladcp\AMK71\dNNN directory, where NNNN stands for the CTD cast number, e.g. raw data from cast 2757 were stored in the files d:\ASV50\data\ladcp\v2757m_01.000 and v2757s_01..000.

The configuration files (named Mconf.txt and Sconf.txt) containing the operating instructions (setting of track mode, bin depth, etc.) given to the LADCP previously to deployment was stored in the same directory.

Text files of the form NNNNm.log and NNNNs.log are the log of the 'bbtalk' session (testing the state and functioning of the instrument) previous to deployment. The details of the sessions for every single cast in the cruise are to be found in the cast log sheets.

A whole variety of files were created and manipulated during the different processing stages, and no mention will be made of the majority of them for reasons of clarity. The processing procedure may be summarised in two steps:

1- create CTD pressure, temperature and salinity data file as well as navigation collected every second in order to obtain the best possible estimates of depth and sound velocity. This is done using 'SBE Data Processing software and ConvLADCP Fortran program.
2- use the Gerd Krahmann's standard matlab package (v.10.13) with P. Lherminier's improvements (LPO, IFREMER) to process LADCP and CTD data

References

M. Visbeck 2002 Deep Velocity Profiling using Lowered Acoustic Doppler Current Profiler: Bottom Track and Inverse Solutions J. Atmos. Oceanic Technol. 10, 764-773.

3.4 Surface wave measurements

During the 50th cruise of the R/V Akademik Sergei Vavilov (IO RAS) methodological work was carried out to study the possibilities of remote measurement of wave parameters in the open ocean using the digitized data of the ship's navigation radar simultaneously with the SPOTTER buoy-wave recorder, as well as accompanying ship visual observations. Measurements of the characteristics of wind waves in the open ocean were carried out by receiving (1) signals from sensors transmitting information about the surrounding surface situation from the ship's radar station and multilevel processing of the radar image; (2) signals from the sea surface elevation sensor installed on the buoy-wave recorder; (3) visual observations. Based on a comparison of three independent sources of measurements of wind waves, preliminary statistical and spectral data processing was carried out.

The main result of the work can be read the proof that the ship's navigation radar are in good agreement with the high-precision measurements using the wave buoy. This circumstance opens up prospects for using radars to obtain information about the state of the sea surface in an automatic mode. At present, this is a unique result and has broad prospects for use. The main results are shown in **Fig. 15-16**

. CRUISE LOGISTICS

Mobilization

Mobilization for the cruise took place on the way from Kaliningrad (Russia) to the first station of the cruise. It took two days. The scientific team arrived at the ship on August 5th.

ACKNOWLEDGEMENTS

The principal scientists would like to thank the Master, officers, crew and scientists of the RV Akademik Sergey Vavilov for making this such an enjoyable, as well as successful cruise.

TABLES

Table 1. CTD casts

FIGURES

Fig. l Station locations (red circles).

Fig.2 Vertical distribution of oxygen samples along (a) sill sections (b) the 59.5 section.

Fig. 3. Schematic diagram of the large-scale circulation in the northern North Atlantic compiled from [Schmitz and McCartney, 1993; Schott and Brandt, 2007; Sutherland and Pickart, 2008; Lherminier et al., 2010]. Abbreviations for the main topographic features, currents and water masses are explained in the legend. The nominal locations of the 59.5°N hydrographic section (1997 – present) and sections across the straits between Greenland, Iceland, Faeroe and Shetland Islands (2011 – present) are shown with the solid green lines.

Fig. 4. Oxygen concentrations (ml/l) in the water column (lower panel) as observed in March–October 1997 in four hydrographic sections (upper panel) ending nearby the southern tip of Greenland. A separate oxygen maximum in the LSW layer (1000–2000 m) in the Irminger Sea at 59.5°N strongly implies local convective renewal of LSW before 1997. Adapted from [Falina et al., 2007].

Fig. 5. Warming and salinification in the northern North Atlantic between the mid-1990s and mid-2000s, as observed at 59.5°N. The figure shows the 2006–1997 temperature (°C, left) and salinity (right) differences on isobaric surfaces in the Irminger Sea and Iceland Basin. Adapted from [Sarafanov et al., 2007].

Fig. 6. Coherence of the decadal salinity changes (1950s – 2000s) of the intermediate (LSW) and deep (ISOW) waters in the northern North Atlantic and their link to the North Atlantic Oscillation (NAO) index. **(a)** Schematic representation of the LSW and ISOW pathways and locations of the Icelandic Low (L) and Azores High (H) centers constituting the NAO dipole pattern. The red dotted line indicates the 59.5°N transatlantic section. **(b)** Salinity time series for LSW in the Labrador Sea [Yashayaev, 2007] and ISOW in the Iceland basin [Boessenkool et al., 2007; Sarafanov et al., 2007] overlaid by the third order polynomial fits. **(c)** Time series of the winter NAO index, after [Hurrell, 1995], overlaid by 7-year running mean and third order polynomial fit. **(d)** Mechanism of the NAO effect on the decadal changes in temperature (T) and salinity (S) of the northern North Atlantic intermediate and deep waters. Positive / negative links shown with the dark / light grey arrows mean that changes in 'causative' and 'consequential' characteristics have the same / opposite sign(s). The overall effect of the NAO on T and S of the in the water column is negative: persistent NAO decline leads to warming and salinification of the water masses and vice versa, as shown in (b) and (c). Adapted from [Sarafanov, 2009].

Fig. 7. Schematic representation of the upper-ocean circulation and convection intensity in the northern North Atlantic under high (left) and low (right) NAO conditions. Blue (magenta) solid

arrows indicate the upper-ocean flows with higher fraction of colder fresher subpolar (warmer saltier subtropical) waters. The main pathways of the Nordic overflow-derived deep waters are shown with the dotted curves. "C" and "E" symbols are used to denote, respectively, the deep convection sites and the domain, where the Atlantic waters are entrained into ISOW. Larger (smaller) circles indicate stronger (weaker) convection. SPG and STG – the subpolar and subtropical gyres, respectively. Adapted from [Sarafanov, 2009].

Fig. 8. The Deep Western Boundary Current (DWBC) transport variability and its link to the convection intensity in the Labrador Sea. **(a)** Locations of the hydrographic sections (1991–2007) and schematic of the deep water circulation in the Irminger Sea. **(b)** The DWBC transport anomalies at Cape Farewell in 1991–2007, 1 Sv = 10^6 m^3 s^{-1}. The 1994–1997 and 2000–2007 mean anomalies and the 1994–2007 linear trend are shown. **(c)** Anomalies of the DWBC transport at Cape Farewell and the Labrador Sea Water (LSW) thickness in the Labrador Sea in the 1950s–2000s. **(d)** Correlation coefficient (R^2) for the two times series shown in **(c)** at the 0–5-year lag, the LSW thickness leads. The correlation maximum is achieved at the 1–3-year lag. The DWBC transport anomalies in the southern Irminger Sea are foregone by the convection intensity anomalies in the Labrador Sea. Adapted from [Sarafanov et al., 2009].

Fig. 9. Schematic diagram of the Meridional Overturning Circulation (MOC) at the northern periphery of the Atlantic Ocean, northeast of Cape Farewell. The dotted lines refer to the σ_0 isopycnals 27.55 and 27.80. The arrows denote the integral meridional and diapycnal volume fluxes. Where the signs are specified, the positive (negative) transports are northward (southward). The NAC and EGIC transports in the upper layer ($\sigma_0 < 27.55$) at 59.5°N are the throughputs accounting for the recirculations. EGIC – the East Greenland / Irminger Current – refers to the upper part of the Western Boundary Current. Other abbreviations are explained in the legend to **Fig. 3**. Adapted from [Sarafanov et al., 2012].

Fig. 10. Salinity observed in the northwestern Irminger Sea at 64.3°N in February 1998. The σ_0 isopycnals 27.55, 27.70, 27.80 and 27.88 are plotted as the thick black lines; the station locations are marked with the ticks on the top axis. The plot shows fresh dense waters descending (cascading) down the continental slope of Greenland down to the LSW layer ($27.70 < \sigma_0 < 27.80$) and the layer of the Nordic Seas overflow-derived deep waters ($\sigma_0 > 27.80$). Adapted from [Falina et al., 2012].

Fig. 11. 3-minute atmospheric pressure (mb) measured during 50 cruise of Akademik Sergey Vavilov.

Fig. 12. 3-minute Air temperature (°C) measured during 50 cruise of Akademik Sergey Vavilov.

Table 1

R/V AK. SERGEY VAVILOV CRUISE 50

STA	DATE	TIME		POSITION		DEPTH	ABV	N BOTTLES	
2756	081020	1124	BE	59 30.0 N	005 18.0 W	111	3	7	CTD,LADCP,O2
2756	081020	1130	BO	59 29.9 N	005 18.0 W	111	3	7	CTD,LADCP,O2
2756	081020	1146	EN	59 29.9 N	005 18.2 W	111	3	7	CTD,LADCP,O2
2757	081020	1408	BE	59 30.0 N	005 59.9 W	140	3	7	CTD,LADCP,O2
2757	081020	1414	BO	59 29.9 N	005 59.9 W	140	3	7	CTD,LADCP,O2
2757	081020	1431	EN	59 29.9 N	005 59.9 W	140	3	7	CTD,LADCP,O2
2758	081020	1659	BE	59 30.0 N	006 39.9 W	576	5	14	CTD,LADCP,O2
2758	081020	1716	BO	59 30.0 N	006 39.9 W	576	5	14	CTD,LADCP,O2
2758	081020	1740	EN	59 30.0 N	006 40.0 W	576	5	14	CTD,LADCP,O2
2759	081020	1959	BE	59 30.0 N	007 19.8 W	1054	3	20	CTD,LADCP,O2
2759	081020	2022	BO	59 30.0 N	007 19.8 W	1054	3	20	CTD,LADCP,O2
2759	081020	2059	EN	59 30.0 N	007 19.8 W	1054	3	20	CTD,LADCP,O2
2760	081020	2328	BE	59 30.0 N	007 59.8 W	1129	5	20	CTD,LADCP,O2
2760	081020	2353	BO	59 30.0 N	007 59.9 W	1129	5	20	CTD,LADCP,O2
2760	081120	0030	EN	59 30.0 N	007 59.9 W	1129	5	20	CTD,LADCP,O2
2761	081120	0257	BE	59 30.0 N	008 39.8 W	1384	5	20	CTD,LADCP,O2
2761	081120	0329	BO	59 29.9 N	008 39.9 W	1384	5	20	CTD,LADCP,O2
2761	081120	0411	EN	59 29.9 N	008 39.9 W	1384	5	20	CTD,LADCP,O2
2762	081120	0636	BE	59 29.9 N	009 19.6 W	1489	4	21	CTD,LADCP,O2
2762	081120	0711	BO	59 29.9 N	009 20.0 W	1489	4	21	CTD,LADCP,O2
2762	081120	0755	EN	59 29.9 N	009 20.0 W	1489	4	21	CTD,LADCP,O2
2763	081120	1014	BE	59 30.0 N	010 00.0 W	1035	4	20	CTD,LADCP,O2
2763	081120	1040	BO	59 30.0 N	010 00.0 W	1035	4	20	CTD,LADCP,O2
2763	081120	1116	EN	59 30.0 N	010 00.0 W	1035	4	20	CTD,LADCP,O2
2764	081120	1407	BE	59 30.0 N	010 39.4 W	1549	5	21	CTD,LADCP,O2
2764	081120	1443	BO	59 29.9 N	010 39.9 W	1549	5	21	CTD,LADCP,O2
2764	081120	1527	EN	59 29.9 N	010 39.9 W	1549	5	21	CTD,LADCP,O2
2765	081120	1756	BE	59 30.0 N	011 19.8 W	1627	5	19	CTD,LADCP,O2
2765	081120	1830	BO	59 29.9 N	011 20.0 W	1627	5	19	CTD,LADCP,O2
2765	081120	1917	EN	59 29.9 N	011 20.0 W	1627	5	19	CTD,LADCP,O2
2766	081120	2141	BE	59 30.0 N	012 00.0 W	1504	7	21	CTD,LADCP,O2
2766	081120	2215	BO	59 29.9 N	011 59.9 W	1504	7	21	CTD,LADCP,O2
2766	081120	2301	EN	59 29.9 N	011 59.9 W	1504	7	21	CTD,LADCP,O2
2767	081220	0120	BE	59 30.0 N	012 39.9 W	1362	8	19	CTD,LADCP,O2
2767	081220	0151	BO	59 30.0 N	012 40.0 W	1362	8	19	CTD,LADCP,O2
2767	081220	0229	EN	59 30.0 N	012 40.0 W	1362	8	19	CTD,LADCP,O2
2768	081220	0504	BE	59 29.9 N	013 19.9 W	1292	4	20	CTD,LADCP,O2
2768	081220	0529	BO	59 29.9 N	013 19.9 W	1292	4	20	CTD,LADCP,O2
2768	081220	0608	EN	59 29.9 N	013 19.9 W	1292	4	20	CTD,LADCP,O2
2769	081220	0829	BE	59 30.0 N	014 00.0 W	1000	5	19	CTD,LADCP,O2
2769	081220	0854	BO	59 29.9 N	014 00.0 W	1000	5	19	CTD,LADCP,O2
2769	081220	0932	EN	59 29.9 N	014 00.0 W	1000	5	19	CTD,LADCP,O2
2770	081220	1154	BE	59 30.0 N	014 39.9 W	1001	4	19	CTD,LADCP,O2
2770	081220	1219	BO	59 30.0 N	014 39.9 W	1001	4	19	CTD,LADCP,O2
2770	081220	1255	EN	59 30.0 N	014 39.9 W	1001	4	19	CTD,LADCP,O2
2771	081220	1525	BE	59 29.9 N	015 19.5 W	1518	3	19	CTD,LADCP,O2
2771	081220	1602	BO	59 30.0 N	015 19.7 W	1518	3	19	CTD,LADCP,O2
2771	081220	1646	EN	59 29.9 N	015 19.7 W	1518	3	19	CTD,LADCP,O2
2772	081220	1956	BE	59 30.0 N	015 59.9 W	1561	5	20	CTD,LADCP,O2
2772	081220	2029	BO	59 29.9 N	016 00.0 W	1561	5	20	CTD,LADCP,O2
2772	081220	2115	EN	59 29.9 N	016 00.0 W	1561	5	20	CTD,LADCP,O2
2773	081220	2338	BE	59 30.0 N	016 39.9 W	1087	6	0	CTD,LADCP,O2

2773	081320	0005	BO	59 29.9 N	016 39.9 W	1087	6	0	CTD,LADCP,O2
2773	081320	0007	EN	59 29.9 N	016 39.9 W	1087	6	0	CTD,LADCP,O2
2773a	081320	0008	BE	59 29.9 N	016 39.9 W	1086	5	18	CTD,LADCP,O2
2773a	081320	0008	BO	59 29.9 N	016 39.9 W	1086	5	18	CTD,LADCP,O2
2773a	081320	0042	EN	59 29.9 N	016 39.9 W	1086	5	18	CTD,LADCP,O2
2774	081320	0305	BE	59 29.9 N	017 19.8 W	1769	6	21	CTD,LADCP,O2
2774	081320	0344	BO	59 29.9 N	017 19.8 W	1769	6	21	CTD,LADCP,O2
2774	081320	0434	EN	59 29.9 N	017 19.8 W	1769	6	21	CTD,LADCP,O2
2775	081320	0706	BE	59 30.0 N	017 59.9 W	2220	3	21	CTD,LADCP,O2
2775	081320	0749	BO	59 29.9 N	017 59.9 W	2220	3	21	CTD,LADCP,O2
2775	081320	0852	EN	59 29.9 N	017 59.9 W	2220	3	21	CTD,LADCP,O2
2776	081320	1132	BE	59 30.0 N	018 39.9 W	2780	5	21	CTD,LADCP,O2
2776	081320	1227	BO	59 29.9 N	018 40.0 W	2780	5	21	CTD,LADCP,O2
2776	081320	1334	EN	59 29.9 N	018 40.0 W	2780	5	21	CTD,LADCP,O2
2777	081320	1604	BE	59 30.0 N	019 19.6 W	2704	4	21	CTD,LADCP,O2
2777	081320	1701	BO	59 29.9 N	019 19.9 W	2704	4	21	CTD,LADCP,O2
2777	081320	1804	EN	59 29.9 N	019 19.9 W	2704	4	21	CTD,LADCP,O2
2778	081320	2145	BE	59 30.0 N	019 59.9 W	2809	4	21	CTD,LADCP,O2
2778	081320	2243	BO	59 29.9 N	019 59.9 W	2809	4	21	CTD,LADCP,O2
2778	081320	2348	EN	59 29.9 N	019 59.9 W	2809	4	21	CTD,LADCP,O2
2779	081420	0238	BE	59 30.0 N	020 39.8 W	2827	5	21	CTD,LADCP,O2
2779	081420	0338	BO	59 29.9 N	020 39.9 W	2827	5	21	CTD,LADCP,O2
2779	081420	0443	EN	59 29.9 N	020 39.9 W	2827	5	21	CTD,LADCP,O2
2780	081420	0726	BE	59 30.0 N	021 19.9 W	2903	4	21	CTD,LADCP,O2
2780	081420	0822	BO	59 30.0 N	021 20.0 W	2903	4	21	CTD,LADCP,O2
2780	081420	0927	EN	59 30.0 N	021 20.0 W	2903	4	21	CTD,LADCP,O2
2781	081420	1206	BE	59 30.0 N	021 59.9 W	2743	4	21	CTD,LADCP,O2
2781	081420	1258	BO	59 29.9 N	022 00.0 W	2743	4	21	CTD,LADCP,O2
2781	081420	1401	EN	59 29.9 N	021 59.9 W	2743	4	21	CTD,LADCP,O2
2782	081420	1641	BE	59 30.0 N	022 39.8 W	2458	4	21	CTD,LADCP,O2
2782	081420	1731	BO	59 30.0 N	022 39.9 W	2458	4	21	CTD,LADCP,O2
2782	081420	1833	EN	59 30.0 N	022 39.9 W	2458	4	21	CTD,LADCP,O2
2783	081420	2206	BE	59 30.0 N	023 19.9 W	2435	9	21	CTD,LADCP,O2
2783	081420	2257	BO	59 30.0 N	023 19.9 W	2435	9	21	CTD,LADCP,O2
2783	081420	2350	EN	59 30.0 N	023 20.0 W	2435	9	21	CTD,LADCP,O2
2784	081520	0235	BE	59 30.0 N	023 59.8 W	2569	5	21	CTD,LADCP,O2
2784	081520	0325	BO	59 30.0 N	023 59.9 W	2569	5	21	CTD,LADCP,O2
2784	081520	0427	EN	59 30.0 N	023 59.9 W	2569	5	21	CTD,LADCP,O2
2785	081520	0711	BE	59 30.0 N	024 39.7 W	2562	7	20	CTD,LADCP,O2
2785	081520	0802	BO	59 30.0 N	024 39.9 W	2562	7	20	CTD,LADCP,O2
2785	081520	0901	EN	59 30.0 N	024 40.0 W	2562	7	20	CTD,LADCP,O2
2786	081520	1149	BE	59 30.0 N	025 19.9 W	2494	9	21	CTD,LADCP,O2
2786	081520	1238	BO	59 30.0 N	025 19.9 W	2494	9	21	CTD,LADCP,O2
2786	081520	1336	EN	59 30.0 N	025 19.9 W	2494	9	21	CTD,LADCP,O2
2787	081520	1623	BE	59 30.0 N	025 59.9 W	2305	3	21	CTD,LADCP,O2
2787	081520	1708	BO	59 30.0 N	025 59.9 W	2305	3	21	CTD,LADCP,O2
2787	081520	1808	EN	59 30.0 N	025 59.9 W	2305	3	21	CTD,LADCP,O2
2788	081520	2127	BE	59 30.0 N	026 39.9 W	2236	2	21	CTD,LADCP,O2
2788	081520	2212	BO	59 30.0 N	026 39.9 W	2236	2	21	CTD,LADCP,O2
2788	081520	2304	EN	59 30.0 N	026 39.8 W	2236	2	21	CTD,LADCP,O2
2789	081620	0146	BE	59 30.0 N	027 19.9 W	1905	5	21	CTD,LADCP,O2
2789	081620	0225	BO	59 30.0 N	027 20.0 W	1905	5	21	CTD,LADCP,O2
2789	081620	0314	EN	59 30.0 N	027 20.0 W	1905	5	21	CTD,LADCP,O2
2790	081620	0551	BE	59 30.0 N	027 59.8 W	1970	5	21	CTD,LADCP,O2
2790	081620	0633	BO	59 29.9 N	027 59.9 W	1970	5	21	CTD,LADCP,O2

2790	081620	0722	EN	59 30.0 N	027 59.9 W	1970	5	21	CTD,LADCP,O2
2791	081620	0955	BE	59 29.9 N	028 39.9 W	1725	9	21	CTD,LADCP,O2
2791	081620	1031	BO	59 29.9 N	028 39.9 W	1725	9	21	CTD,LADCP,O2
2791	081620	1116	EN	59 29.9 N	028 39.9 W	1725	9	21	CTD,LADCP,O2
2792	081620	1329	BE	59 30.0 N	029 19.4 W	1426	9	19	CTD,LADCP,O2
2792	081620	1402	BO	59 29.9 N	029 20.0 W	1426	9	19	CTD,LADCP,O2
2792	081620	1440	EN	59 29.9 N	029 20.0 W	1426	9	19	CTD,LADCP,O2
2793	081620	1738	BE	59 30.0 N	029 59.9 W	1494	8	19	CTD,LADCP,O2
2793	081620	1813	BO	59 30.0 N	029 59.9 W	1494	8	19	CTD,LADCP,O2
2793	081620	1851	EN	59 29.9 N	029 59.9 W	1494	8	19	CTD,LADCP,O2
2794	081620	2114	BE	59 30.0 N	030 40.0 W	1527	3	19	CTD,LADCP,O2
2794	081620	2146	BO	59 29.9 N	030 39.9 W	1527	3	19	CTD,LADCP,O2
2794	081620	2225	EN	59 29.9 N	030 39.9 W	1527	3	19	CTD,LADCP,O2
2795	081720	0047	BE	59 29.9 N	031 19.9 W	1725	5	21	CTD,LADCP,O2
2795	081720	0122	BO	59 29.9 N	031 19.7 W	1725	5	21	CTD,LADCP,O2
2795	081720	0207	EN	59 29.9 N	031 19.4 W	1725	5	21	CTD,LADCP,O2
2796	081720	0436	BE	59 30.0 N	031 59.9 W	1921	5	20	CTD,LADCP,O2
2796	081720	0516	BO	59 29.9 N	032 00.0 W	1921	5	20	CTD,LADCP,O2
2796	081720	0608	EN	59 29.9 N	031 59.9 W	1921	5	20	CTD,LADCP,O2
2797	081720	0825	BE	59 30.0 N	032 39.9 W	2189	3	21	CTD,LADCP,O2
2797	081720	0910	BO	59 30.0 N	032 40.0 W	2189	3	21	CTD,LADCP,O2
2797	081720	1005	EN	59 30.0 N	032 40.0 W	2189	3	21	CTD,LADCP,O2
2798	081720	1253	BE	59 29.9 N	033 19.7 W	2222	6	21	CTD,LADCP,O2
2798	081720	1337	BO	59 29.9 N	033 20.0 W	2222	6	21	CTD,LADCP,O2
2798	081720	1430	EN	59 29.9 N	033 20.0 W	2222	6	21	CTD,LADCP,O2
2799	081720	1644	BE	59 30.0 N	033 59.8 W	2548	9	21	CTD,LADCP,O2
2799	081720	1733	BO	59 29.9 N	034 00.1 W	2548	9	21	CTD,LADCP,O2
2799	081720	1834	EN	59 29.9 N	034 00.1 W	2548	9	21	CTD,LADCP,O2
2800	081720	2043	BE	59 29.9 N	034 39.9 W	2803	4	21	CTD,LADCP,O2
2800	081720	2139	BO	59 29.9 N	034 40.0 W	2803	4	21	CTD,LADCP,O2
2800	081720	2243	EN	59 30.0 N	034 39.9 W	2803	4	21	CTD,LADCP,O2
2801	081820	0028	BE	59 29.9 N	035 09.8 W	3105	4	21	CTD,LADCP,O2
2801	081820	0129	BO	59 29.9 N	035 09.9 W	3105	4	21	CTD,LADCP,O2
2801	081820	0239	EN	59 29.9 N	035 09.9 W	3105	4	21	CTD,LADCP,O2
2802	081820	0534	BE	59 29.9 N	035 59.9 W	3093	5	21	CTD,LADCP,O2
2802	081820	0632	BO	59 29.9 N	036 00.0 W	3093	5	21	CTD,LADCP,O2
2802	081820	0743	EN	59 29.9 N	036 00.0 W	3093	5	21	CTD,LADCP,O2
2803	081820	1002	BE	59 29.9 N	036 40.0 W	3097	2	21	CTD,LADCP,O2
2803	081820	1059	BO	59 29.9 N	036 40.0 W	3097	2	21	CTD,LADCP,O2
2803	081820	1207	EN	59 29.9 N	036 40.0 W	3097	2	21	CTD,LADCP,O2
2804	081820	1450	BE	59 29.9 N	037 20.0 W	3154	6	21	CTD,LADCP,O2
2804	081820	1547	BO	59 30.0 N	037 20.0 W	3154	6	21	CTD,LADCP,O2
2804	081820	1658	EN	59 30.0 N	037 20.0 W	3154	6	21	CTD,LADCP,O2
2805	081820	1906	BE	59 30.0 N	037 59.9 W	3117	4	21	CTD,LADCP,O2
2805	081820	2005	BO	59 30.0 N	038 00.0 W	3117	4	21	CTD,LADCP,O2
2805	081820	2114	EN	59 29.9 N	038 00.0 W	3117	4	21	CTD,LADCP,O2
2806	081820	2333	BE	59 29.9 N	038 39.9 W	3049	7	21	CTD,LADCP,O2
2806	081920	0030	BO	59 30.0 N	038 39.9 W	3049	7	21	CTD,LADCP,O2
2806	081920	0138	EN	59 30.0 N	038 40.0 W	3049	7	21	CTD,LADCP,O2
2807	081920	0359	BE	59 30.0 N	039 19.9 W	2975	6	21	CTD,LADCP,O2
2807	081920	0453	BO	59 30.0 N	039 19.9 W	2975	6	21	CTD,LADCP,O2
2807	081920	0600	EN	59 30.1 N	039 19.9 W	2975	6	21	CTD,LADCP,O2
2808	081920	0816	BE	59 29.9 N	040 00.0 W	2889	5	21	CTD,LADCP,O2
2808	081920	0911	BO	59 29.9 N	040 00.0 W	2889	5	21	CTD,LADCP,O2
2808	081920	1016	EN	59 29.9 N	040 00.0 W	2889	5	21	CTD,LADCP,O2

2809	081920	1129	BE	59 29.9 N	040 20.0 W	2670	4	21	CTD,LADCP,O2
2809	081920	1219	BO	59 29.9 N	040 20.0 W	2670	4	21	CTD,LADCP,O2
2809	081920	1320	EN	59 29.9 N	040 20.0 W	2670	4	21	CTD,LADCP,O2
2810	081920	1500	BE	59 29.9 N	040 39.9 W	2582	3	21	CTD,LADCP,O2
2810	081920	1547	BO	59 29.9 N	040 39.9 W	2582	3	21	CTD,LADCP,O2
2810	081920	1648	EN	59 30.0 N	040 40.0 W	2582	3	21	CTD,LADCP,O2
2811	081920	1808	BE	59 34.0 N	041 00.0 W	2399	3	21	CTD,LADCP,O2
2811	081920	1855	BO	59 33.8 N	041 00.4 W	2399	3	21	CTD,LADCP,O2
2811	081920	1950	EN	59 33.5 N	041 00.9 W	2399	3	21	CTD,LADCP,O2
2812	081920	2100	BE	59 38.8 N	041 15.6 W	2208	9	21	CTD,LADCP,O2
2812	081920	2144	BO	59 38.6 N	041 15.8 W	2208	9	21	CTD,LADCP,O2
2812	081920	2237	EN	59 38.4 N	041 16.0 W	2208	9	21	CTD,LADCP,O2
2813	081920	2348	BE	59 42.8 N	041 31.6 W	1999	5	21	CTD,LADCP,O2
2813	082020	0030	BO	59 42.7 N	041 31.7 W	1999	5	21	CTD,LADCP,O2
2813	082020	0121	EN	59 42.6 N	041 31.8 W	1999	5	21	CTD,LADCP,O2
2814	082020	0227	BE	59 46.5 N	041 46.9 W	1833	5	18	CTD,LADCP,O2
2814	082020	0305	BO	59 46.6 N	041 47.1 W	1833	5	18	CTD,LADCP,O2
2814	082020	0351	EN	59 46.6 N	041 47.0 W	1833	5	18	CTD,LADCP,O2
2815	082020	0435	BE	59 48.6 N	041 55.5 W	1760	4	17	CTD,LADCP,O2
2815	082020	0511	BO	59 48.5 N	041 55.8 W	1760	4	17	CTD,LADCP,O2
2815	082020	0554	EN	59 48.4 N	041 56.1 W	1760	4	17	CTD,LADCP,O2
2816	082020	0633	BE	59 50.7 N	042 03.3 W	1633	3	15	CTD,LADCP,O2
2816	082020	0708	BO	59 50.6 N	042 03.8 W	1633	3	15	CTD,LADCP,O2
2816	082020	0749	EN	59 50.3 N	042 04.5 W	1633	3	15	CTD,LADCP,O2
2817	082020	0813	BE	59 51.5 N	042 06.4 W	1559	4	14	CTD,LADCP,O2
2817	082020	0843	BO	59 51.2 N	042 07.0 W	1559	4	14	CTD,LADCP,O2
2817	082020	0920	EN	59 50.9 N	042 07.7 W	1559	4	14	CTD,LADCP,O2
2818	082020	0941	BE	59 52.4 N	042 08.7 W	1449	3	12	CTD,LADCP,O2
2818	082020	1012	BO	59 52.2 N	042 09.4 W	1449	3	12	CTD,LADCP,O2
2818	082020	1046	EN	59 51.9 N	042 10.0 W	1449	3	12	CTD,LADCP,O2
2819	082020	1122	BE	59 52.9 N	042 11.9 W	810	2	11	CTD,LADCP,O2
2819	082020	1147	BO	59 52.9 N	042 12.4 W	810	2	11	CTD,LADCP,O2
2819	082020	1209	EN	59 52.8 N	042 12.6 W	810	2	11	CTD,LADCP,O2
2820	082020	1234	BE	59 53.5 N	042 15.5 W	382	5	9	CTD,LADCP,O2
2820	082020	1243	BO	59 53.5 N	042 15.6 W	382	5	9	CTD,LADCP,O2
2820	082020	1257	EN	59 53.5 N	042 15.6 W	382	5	9	CTD,LADCP,O2
2821	082020	1315	BE	59 53.8 N	042 18.6 W	325	3	8	CTD,LADCP,O2
2821	082020	1331	BO	59 54.0 N	042 19.2 W	325	3	8	CTD,LADCP,O2
2821	082020	1343	EN	59 53.9 N	042 19.2 W	325	3	8	CTD,LADCP,O2
2822	082020	1443	BE	59 54.1 N	042 22.7 W	231	3	7	CTD,LADCP,O2
2822	082020	1452	BO	59 54.2 N	042 22.7 W	231	3	7	CTD,LADCP,O2
2822	082020	1506	EN	59 54.2 N	042 22.8 W	231	3	7	CTD,LADCP,O2
2823	082020	1527	BE	59 54.3 N	042 26.2 W	217	3	7	CTD,LADCP,O2
2823	082020	1538	BO	59 54.4 N	042 26.4 W	217	3	7	CTD,LADCP,O2
2823	082020	1550	EN	59 54.4 N	042 26.4 W	217	3	7	CTD,LADCP,O2
2824	082020	1613	BE	59 54.6 N	042 30.0 W	201	4	7	CTD,LADCP,O2
2824	082020	1621	BO	59 54.5 N	042 30.0 W	201	4	7	CTD,LADCP,O2
2824	082020	1632	EN	59 54.5 N	042 30.1 W	201	4	7	CTD,LADCP,O2
2825	082020	1652	BE	59 54.8 N	042 33.5 W	186	5	6	CTD,LADCP,O2
2825	082020	1700	BO	59 54.8 N	042 33.6 W	186	5	6	CTD,LADCP,O2
2825	082020	1711	EN	59 54.7 N	042 33.7 W	186	5	6	CTD,LADCP,O2
2826	082020	1731	BE	59 55.1 N	042 37.1 W	184	4	6	CTD,LADCP,O2
2826	082020	1740	BO	59 55.2 N	042 37.3 W	184	4	6	CTD,LADCP,O2
2826	082020	1751	EN	59 55.1 N	042 37.5 W	184	4	6	CTD,LADCP,O2
2827	082020	1810	BE	59 55.6 N	042 40.8 W	194	3	6	CTD,LADCP,O2

2827	082020	1818	BO	59 55.6 N	042 40.9 W	194	3	6	CTD,LADCP,O2
2827	082020	1830	EN	59 55.5 N	042 41.0 W	194	3	6	CTD,LADCP,O2
2828	082020	1847	BE	59 55.6 N	042 44.2 W	192	4	6	CTD,LADCP,O2
2828	082020	1857	BO	59 55.7 N	042 44.5 W	192	4	6	CTD,LADCP,O2
2828	082020	1908	EN	59 55.6 N	042 44.7 W	192	4	6	CTD,LADCP,O2
2829	082020	1926	BE	59 56.2 N	042 47.9 W	185	4	6	CTD,LADCP,O2
2829	082020	1935	BO	59 56.2 N	042 48.1 W	185	4	6	CTD,LADCP,O2
2829	082020	1947	EN	59 56.1 N	042 48.5 W	185	4	6	CTD,LADCP,O2
2830	082020	2008	BE	59 56.2 N	042 51.8 W	170	5	7	CTD,LADCP,O2
2830	082020	2015	BO	59 56.1 N	042 52.0 W	170	5	7	CTD,LADCP,O2
2830	082020	2029	EN	59 56.0 N	042 52.5 W	170	5	7	CTD,LADCP,O2
2831	082020	2047	BE	59 56.8 N	042 55.2 W	170	5	7	CTD,LADCP,O2
2831	082020	2108	BO	59 56.4 N	042 55.9 W	170	5	7	CTD,LADCP,O2
2831	082020	2117	EN	59 56.2 N	042 56.2 W	170	5	7	CTD,LADCP,O2
2832	082020	2138	BE	59 57.3 N	042 58.9 W	168	4	7	CTD,LADCP,O2
2832	082020	2150	BO	59 57.2 N	042 59.3 W	168	4	7	CTD,LADCP,O2
2832	082020	2202	EN	59 57.0 N	042 59.7 W	168	4	7	CTD,LADCP,O2
2833	082220	1339	BE	55 48.1 N	034 28.6 W	2144	8	21	CTD,LADCP,O2
2833	082220	1425	BO	55 48.0 N	034 28.4 W	2144	8	21	CTD,LADCP,O2
2833	082220	1518	EN	55 48.0 N	034 28.4 W	2144	8	21	CTD,LADCP,O2
2834	082220	1743	BE	56 03.0 N	034 17.1 W	1675	4	21	CTD,LADCP,O2
2834	082220	1816	BO	56 03.0 N	034 17.0 W	1675	4	21	CTD,LADCP,O2
2834	082220	1900	EN	56 03.1 N	034 17.0 W	1675	4	21	CTD,LADCP,O2
2835	082220	2136	BE	56 24.0 N	034 01.3 W	1735	5	20	CTD,LADCP,O2
2835	082220	2210	BO	56 23.9 N	034 01.4 W	1735	5	20	CTD,LADCP,O2
2835	082220	2254	EN	56 24.0 N	034 01.7 W	1735	5	20	CTD,LADCP,O2
2836	082320	0132	BE	56 42.0 N	033 37.6 W	1767	9	15	CTD,LADCP,O2
2836	082320	0209	BO	56 42.0 N	033 37.5 W	1767	9	15	CTD,LADCP,O2
2836	082320	0252	EN	56 42.0 N	033 37.5 W	1767	9	15	CTD,LADCP,O2
2837	082320	0317	BE	56 42.6 N	033 36.9 W	2131	2	15	CTD,LADCP,O2
2837	082320	0359	BO	56 42.6 N	033 37.0 W	2131	2	15	CTD,LADCP,O2
2837	082320	0448	EN	56 42.5 N	033 37.0 W	2131	2	15	CTD,LADCP,O2
2838	082320	0515	BE	56 43.5 N	033 35.6 W	2424	5	16	CTD,LADCP,O2
2838	082320	0559	BO	56 43.4 N	033 35.6 W	2424	5	16	CTD,LADCP,O2
2838	082320	0652	EN	56 43.4 N	033 35.6 W	2424	5	16	CTD,LADCP,O2
2839	082320	0722	BE	56 45.1 N	033 33.5 W	2208	9	15	CTD,LADCP,O2
2839	082320	0803	BO	56 45.1 N	033 33.5 W	2208	9	15	CTD,LADCP,O2
2839	082320	0853	EN	56 45.1 N	033 33.5 W	2208	9	15	CTD,LADCP,O2
2840	082320	0917	BE	56 46.0 N	033 32.3 W	2025	3	14	CTD,LADCP,O2
2840	082320	0957	BO	56 46.0 N	033 32.3 W	2025	3	14	CTD,LADCP,O2
2840	082320	1043	EN	56 46.0 N	033 32.4 W	2025	3	14	CTD,LADCP,O2
2841	082320	1104	BE	56 46.7 N	033 31.5 W	1747	3	15	CTD,LADCP,O2
2841	082320	1140	BO	56 46.7 N	033 31.5 W	1747	3	15	CTD,LADCP,O2
2841	082320	1223	EN	56 46.7 N	033 31.5 W	1747	3	15	CTD,LADCP,O2
2842	082320	1346	BE	56 50.9 N	033 26.1 W	1916	5	16	CTD,LADCP,O2
2842	082320	1425	BO	56 50.9 N	033 26.0 W	1916	5	16	CTD,LADCP,O2
2842	082320	1509	EN	56 50.9 N	033 25.9 W	1916	5	16	CTD,LADCP,O2
2843	082320	1550	BE	56 54.5 N	033 21.3 W	1951	9	16	CTD,LADCP,O2
2843	082320	1631	BO	56 54.6 N	033 21.1 W	1951	9	16	CTD,LADCP,O2
2843	082320	1714	EN	56 54.7 N	033 20.9 W	1951	9	16	CTD,LADCP,O2
2845	082320	2202	BE	57 18.5 N	032 49.3 W	1362	3	18	CTD,LADCP,O2
2845	082320	2233	BO	57 18.6 N	032 49.3 W	1362	3	18	CTD,LADCP,O2
2845	082320	2309	EN	57 18.6 N	032 49.3 W	1362	3	18	CTD,LADCP,O2
2846	082420	0126	BE	57 34.7 N	032 28.5 W	1740	8	19	CTD,LADCP,O2
2846	082420	0201	BO	57 34.7 N	032 28.6 W	1740	8	19	CTD,LADCP,O2

2846	082420	0245	EN	57 34.7 N	032 28.6 W	1740	8	19	CTD,LADCP,O2
2847	082420	0512	BE	57 52.7 N	032 07.1 W	1426	6	14	CTD,LADCP,O2
2847	082420	0544	BO	57 52.8 N	032 07.0 W	1426	6	14	CTD,LADCP,O2
2847	082420	0618	EN	57 52.7 N	032 07.0 W	1426	6	14	CTD,LADCP,O2
2848	082420	0851	BE	58 11.9 N	031 44.9 W	1599	5	18	CTD,LADCP,O2
2848	082420	0925	BO	58 12.0 N	031 44.9 W	1599	5	18	CTD,LADCP,O2
2848	082420	1007	EN	58 12.0 N	031 45.0 W	1599	5	18	CTD,LADCP,O2
2849	082420	1239	BE	58 31.7 N	031 25.3 W	1703	7	17	CTD,LADCP,O2
2849	082420	1316	BO	58 31.8 N	031 25.2 W	1703	7	17	CTD,LADCP,O2
2849	082420	1358	EN	58 31.7 N	031 25.2 W	1703	7	17	CTD,LADCP,O2
2850	082420	1652	BE	58 50.7 N	031 16.0 W	1498	5	17	CTD,LADCP,O2
2850	082420	1724	BO	58 50.9 N	031 16.0 W	1498	5	17	CTD,LADCP,O2
2850	082420	1802	EN	58 51.1 N	031 15.7 W	1498	5	17	CTD,LADCP,O2
2851	082420	1952	BE	59 03.0 N	030 57.2 W	1211	5	17	CTD,LADCP,O2
2851	082420	2018	BO	59 03.0 N	030 57.2 W	1211	5	17	CTD,LADCP,O2
2851	082420	2051	EN	59 03.1 N	030 57.2 W	1211	5	17	CTD,LADCP,O2
2852	082420	2300	BE	59 17.9 N	030 34.2 W	1321	10	17	CTD,LADCP,O2
2852	082420	2330	BO	59 18.0 N	030 34.1 W	1321	10	17	CTD,LADCP,O2
2852	082520	0004	EN	59 18.0 N	030 34.1 W	1321	10	17	CTD,LADCP,O2
2853	082520	0214	BE	59 32.9 N	030 11.1 W	1250	4	15	CTD,LADCP,O2
2853	082520	0239	BO	59 32.9 N	030 11.1 W	1250	4	15	CTD,LADCP,O2
2853	082520	0312	EN	59 32.9 N	030 11.1 W	1250	4	15	CTD,LADCP,O2
2854	082520	0526	BE	59 47.9 N	029 48.4 W	1017	7	13	CTD,LADCP,O2
2854	082520	0550	BO	59 48.0 N	029 48.3 W	1017	7	13	CTD,LADCP,O2
2854	082520	0618	EN	59 48.0 N	029 48.3 W	1017	7	13	CTD,LADCP,O2
2855	082520	0836	BE	60 03.0 N	029 25.2 W	942	2	12	CTD,LADCP,O2
2855	082520	0859	BO	60 03.0 N	029 25.2 W	942	2	12	CTD,LADCP,O2
2855	082520	0925	EN	60 03.0 N	029 25.2 W	942	2	12	CTD,LADCP,O2
2856	082520	1137	BE	60 18.0 N	029 02.3 W	1086	9	12	CTD,LADCP,O2
2856	082520	1204	BO	60 18.0 N	029 02.2 W	1086	9	12	CTD,LADCP,O2
2856	082520	1233	EN	60 17.9 N	029 02.1 W	1086	9	12	CTD,LADCP,O2
2857	082520	1539	BE	60 35.9 N	028 34.7 W	804	5	14	CTD,LADCP,O2
2857	082520	1602	BO	60 36.0 N	028 34.6 W	804	5	14	CTD,LADCP,O2
2857	082520	1624	EN	60 36.0 N	028 34.5 W	804	5	14	CTD,LADCP,O2
2858	082520	1850	BE	60 54.0 N	028 07.3 W	660	4	12	CTD,LADCP,O2
2858	082520	1912	BO	60 54.2 N	028 07.0 W	660	4	12	CTD,LADCP,O2
2858	082520	1932	EN	60 54.2 N	028 07.0 W	660	4	12	CTD,LADCP,O2
2859	082520	2158	BE	61 12.0 N	027 39.4 W	663	4	14	CTD,LADCP,O2
2859	082520	2217	BO	61 12.0 N	027 39.3 W	663	4	14	CTD,LADCP,O2
2859	082520	2238	EN	61 12.0 N	027 39.3 W	663	4	14	CTD,LADCP,O2
2860	082620	0104	BE	61 30.0 N	027 10.5 W	712	5	11	CTD,LADCP,O2
2860	082620	0122	BO	61 29.9 N	027 10.5 W	712	5	11	CTD,LADCP,O2
2860	082620	0143	EN	61 30.0 N	027 10.4 W	712	5	11	CTD,LADCP,O2
2861	082620	0414	BE	61 47.9 N	026 41.4 W	1016	4	14	CTD,LADCP,O2
2861	082620	0439	BO	61 48.0 N	026 41.3 W	1016	4	14	CTD,LADCP,O2
2861	082620	0510	EN	61 47.9 N	026 41.3 W	1016	4	14	CTD,LADCP,O2
2862	082620	0740	BE	62 05.9 N	026 12.3 W	776	2	11	CTD,LADCP,O2
2862	082620	0759	BO	62 05.9 N	026 12.3 W	776	2	11	CTD,LADCP,O2
2862	082620	0822	EN	62 05.9 N	026 12.3 W	776	2	11	CTD,LADCP,O2
2863	082620	1055	BE	62 23.9 N	025 43.3 W	697	4	10	CTD,LADCP,O2
2863	082620	1113	BO	62 24.0 N	025 43.2 W	697	4	10	CTD,LADCP,O2
2863	082620	1133	EN	62 24.0 N	025 43.2 W	697	4	10	CTD,LADCP,O2
2864	082620	1440	BE	62 41.9 N	025 14.2 W	622	6	9	CTD,LADCP,O2
2864	082620	1458	BO	62 42.0 N	025 14.2 W	622	6	9	CTD,LADCP,O2
2864	082620	1517	EN	62 42.0 N	025 14.2 W	622	6	9	CTD,LADCP,O2

2865	082620	1742	BE	62 59.9 N	024 45.1 W	256	3	7	CTD,LADCP,O2
2865	082620	1754	BO	63 00.0 N	024 45.1 W	256	3	7	CTD,LADCP,O2
2865	082620	1803	EN	63 00.0 N	024 45.0 W	256	3	7	CTD,LADCP,O2
2866	082620	2143	BE	63 24.8 N	023 55.2 W	144	3	6	CTD,LADCP,O2
2866	082620	2156	BO	63 24.9 N	023 55.0 W	144	3	6	CTD,LADCP,O2
2866	082620	2208	EN	63 24.9 N	023 55.0 W	144	3	6	CTD,LADCP,O2
2867	082720	1159	BE	65 36.3 N	025 00.5 W	81	4	5	CTD,LADCP,O2
2867	082720	1208	BO	65 36.3 N	025 00.6 W	81	4	5	CTD,LADCP,O2
2867	082720	1219	EN	65 36.3 N	025 00.6 W	81	4	5	CTD,LADCP,O2
2868	082720	1311	BE	65 39.9 N	025 15.4 W	91	4	4	CTD,LADCP,O2
2868	082720	1322	BO	65 39.9 N	025 15.9 W	91	4	4	CTD,LADCP,O2
2868	082720	1332	EN	65 39.9 N	025 15.9 W	91	4	4	CTD,LADCP,O2
2869	082720	1552	BE	65 45.0 N	025 38.5 W	255	4	6	CTD,LADCP,O2
2869	082720	1605	BO	65 45.0 N	025 38.7 W	255	4	6	CTD,LADCP,O2
2869	082720	1614	EN	65 45.0 N	025 38.7 W	255	4	6	CTD,LADCP,O2
2870	082720	1726	BE	65 49.8 N	025 59.5 W	225	4	5	CTD,LADCP,O2
2870	082720	1739	BO	65 49.8 N	025 59.8 W	225	4	5	CTD,LADCP,O2
2870	082720	1748	EN	65 49.8 N	025 59.8 W	225	4	5	CTD,LADCP,O2
2871	082720	1925	BE	65 56.0 N	026 29.4 W	290	5	7	CTD,LADCP,O2
2871	082720	1938	BO	65 56.1 N	026 29.3 W	290	5	7	CTD,LADCP,O2
2871	082720	1949	EN	65 56.1 N	026 29.1 W	290	5	7	CTD,LADCP,O2
2872	082720	2100	BE	66 00.5 N	026 48.3 W	434	4	9	CTD,LADCP,O2
2872	082720	2116	BO	66 00.4 N	026 48.3 W	434	4	9	CTD,LADCP,O2
2872	082720	2131	EN	66 00.4 N	026 48.3 W	434	4	9	CTD,LADCP,O2
2873	082720	2205	BE	66 02.4 N	026 56.6 W	586	4	11	CTD,LADCP,O2
2873	082720	2225	BO	66 02.4 N	026 56.9 W	586	4	11	CTD,LADCP,O2
2873	082720	2245	EN	66 02.2 N	026 57.2 W	586	4	11	CTD,LADCP,O2
2874	082720	2318	BE	66 04.3 N	027 03.9 W	656	4	12	CTD,LADCP,O2
2874	082720	2337	BO	66 04.1 N	027 04.5 W	656	4	12	CTD,LADCP,O2
2874	082720	2358	EN	66 03.9 N	027 04.9 W	656	4	12	CTD,LADCP,O2
2875	082820	0035	BE	66 06.2 N	027 11.1 W	619	4	12	CTD,LADCP,O2
2875	082820	0055	BO	66 06.0 N	027 11.4 W	619	4	12	CTD,LADCP,O2
2875	082820	0116	EN	66 05.9 N	027 11.8 W	619	4	12	CTD,LADCP,O2
2876	082820	0155	BE	66 07.8 N	027 18.0 W	528	2	11	CTD,LADCP,O2
2876	082820	0210	BO	66 07.7 N	027 18.1 W	528	2	11	CTD,LADCP,O2
2876	082820	0228	EN	66 07.7 N	027 18.5 W	528	2	11	CTD,LADCP,O2
2877	082820	0319	BE	66 11.0 N	027 31.4 W	486	5	11	CTD,LADCP,O2
2877	082820	0334	BO	66 10.8 N	027 31.5 W	486	5	11	CTD,LADCP,O2
2877	082820	0350	EN	66 10.8 N	027 31.6 W	486	5	11	CTD,LADCP,O2
2878	082820	0446	BE	66 14.8 N	027 45.2 W	472	5	9	CTD,LADCP,O2
2878	082820	0500	BO	66 14.9 N	027 45.1 W	472	5	9	CTD,LADCP,O2
2878	082820	0515	EN	66 15.0 N	027 45.0 W	472	5	9	CTD,LADCP,O2
2879	082820	0631	BE	66 19.8 N	028 07.9 W	344	4	9	CTD,LADCP,O2
2879	082820	0644	BO	66 19.9 N	028 07.9 W	344	4	9	CTD,LADCP,O2
2879	082820	0658	EN	66 20.1 N	028 07.9 W	344	4	9	CTD,LADCP,O2
2880	082820	0811	BE	66 25.1 N	028 31.2 W	301	4	8	CTD,LADCP,O2
2880	082820	0824	BO	66 25.1 N	028 31.2 W	301	4	8	CTD,LADCP,O2
2880	082820	0837	EN	66 25.0 N	028 31.3 W	301	4	8	CTD,LADCP,O2
2881	082820	0951	BE	66 30.0 N	028 53.8 W	322	3	11	CTD,LADCP,O2
2881	082820	1006	BO	66 29.9 N	028 54.1 W	322	3	11	CTD,LADCP,O2
2881	082820	1021	EN	66 29.9 N	028 54.1 W	322	3	11	CTD,LADCP,O2
2882	082820	1251	BE	66 35.0 N	029 15.9 W	312	8	12	CTD,LADCP,O2
2882	082820	1305	BO	66 34.9 N	029 16.1 W	312	8	12	CTD,LADCP,O2
2882	082820	1321	EN	66 34.9 N	029 16.2 W	312	8	12	CTD,LADCP,O2
2883	082820	1431	BE	66 39.8 N	029 38.4 W	303	5	11	CTD,LADCP,O2

2883	082820	1445	BO	66 39.8 N	029 38.8 W	303	5	11	CTD,LADCP,O2
2883	082820	1500	EN	66 39.8 N	029 38.8 W	303	5	11	CTD,LADCP,O2
2884	082820	1620	BE	66 45.0 N	030 02.6 W	329	3	12	CTD,LADCP,O2
2884	082820	1634	BO	66 45.0 N	030 02.8 W	329	3	12	CTD,LADCP,O2
2884	082820	1652	EN	66 45.0 N	030 02.9 W	329	3	12	CTD,LADCP,O2
2885	082820	1805	BE	66 49.9 N	030 26.4 W	411	4	13	CTD,LADCP,O2
2885	082820	1822	BO	66 49.9 N	030 26.7 W	411	4	13	CTD,LADCP,O2
2885	082820	1841	EN	66 49.9 N	030 26.5 W	411	4	13	CTD,LADCP,O2
2886	082820	2109	BE	66 55.1 N	030 49.4 W	578	4	15	CTD,LADCP,O2
2886	082820	2129	BO	66 55.1 N	030 49.6 W	578	4	15	CTD,LADCP,O2
2886	082820	2151	EN	66 55.0 N	030 49.7 W	578	4	15	CTD,LADCP,O2
2887	082820	2303	BE	67 00.0 N	031 12.3 W	357	3	11	CTD,LADCP,O2
2887	082820	2318	BO	66 59.9 N	031 12.7 W	357	3	11	CTD,LADCP,O2
2887	082820	2334	EN	66 59.9 N	031 12.6 W	357	3	11	CTD,LADCP,O2
2888	082920	0108	BE	67 04.9 N	031 35.8 W	296	6	10	CTD,LADCP,O2
2888	082920	0118	BO	67 04.8 N	031 35.8 W	296	6	10	CTD,LADCP,O2
2888	082920	0132	EN	67 04.9 N	031 35.7 W	296	6	10	CTD,LADCP,O2
2889	082920	0323	BE	67 09.8 N	031 58.8 W	305	4	10	CTD,LADCP,O2
2889	082920	0335	BO	67 09.9 N	031 59.0 W	305	4	10	CTD,LADCP,O2
2889	082920	0347	EN	67 09.9 N	031 59.0 W	305	4	10	CTD,LADCP,O2
2890	082920	0538	BE	67 15.2 N	032 22.2 W	368	5	10	CTD,LADCP,O2
2890	082920	0552	BO	67 15.2 N	032 22.3 W	368	5	10	CTD,LADCP,O2
2890	082920	0606	EN	67 15.2 N	032 22.2 W	368	5	10	CTD,LADCP,O2
2891	082920	0752	BE	67 20.0 N	032 42.8 W	412	4	13	CTD,LADCP,O2
2891	082920	0809	BO	67 20.0 N	032 43.4 W	412	4	13	CTD,LADCP,O2
2891	082920	0828	EN	67 20.0 N	032 43.4 W	412	4	13	CTD,LADCP,O2
2892	082920	2113	BE	66 25.0 N	28 31.3 W	304	5	21	CTD,LADCP,O2
2892	082920	2124	BO	66 25.0 N	28 31.3 W	304	5	21	CTD,LADCP,O2
2892	082920	2138	EN	66 25.1 N	28 31.0 W	304	5	21	CTD,LADCP,O2
2893	082920	2302	BE	66 19.9 N	28 07.8 W	346	3	10	CTD,LADCP,O2
2893	082920	2313	BO	66 19.9 N	28 07.8 W	346	3	10	CTD,LADCP,O2
2893	082920	2325	EN	66 19.9 N	28 07.9 W	346	3	10	CTD,LADCP,O2
2894	083020	0043	BE	66 14.8 N	27 45.0 W	479	4	12	CTD,LADCP,O2
2894	083020	0057	BO	66 14.8 N	27 45.0 W	479	4	12	CTD,LADCP,O2
2894	083020	0111	EN	66 14.8 N	27 45.0 W	479	4	12	CTD,LADCP,O2
2895	083020	0209	BE	66 10.9 N	27 31.5 W	490	5	12	CTD,LADCP,O2
2895	083020	0223	BO	66 10.9 N	27 31.5 W	490	5	12	CTD,LADCP,O2
2895	083020	0237	EN	66 10.9 N	27 31.5 W	490	5	12	CTD,LADCP,O2
2896	083020	0332	BE	66 07.8 N	27 18.2 W	530	3	13	CTD,LADCP,O2
2896	083020	0347	BO	66 07.8 N	27 18.5 W	530	3	13	CTD,LADCP,O2
2896	083020	0402	EN	66 07.6 N	27 19.0 W	530	3	13	CTD,LADCP,O2
2897	083020	0445	BE	66 06.1 N	27 11.2 W	619	3	13	CTD,LADCP,O2
2897	083020	0502	BO	66 06.1 N	27 11.6 W	619	3	13	CTD,LADCP,O2
2897	083020	0519	EN	66 06.1 N	27 12.2 W	619	3	13	CTD,LADCP,O2
2898	083020	0602	BE	66 04.3 N	27 04.2 W	671	6	15	CTD,LADCP,O2
2898	083020	0619	BO	66 04.3 N	27 04.2 W	671	6	15	CTD,LADCP,O2
2898	083020	0639	EN	66 04.3 N	27 04.2 W	671	6	15	CTD,LADCP,O2
2899	083020	0908	BE	66 03.1 N	026 55.5 W	586	7	14	CTD,LADCP,O2
2899	083020	0933	BO	66 02.6 N	026 56.5 W	586	7	14	CTD,LADCP,O2
2899	083020	1000	EN	66 02.7 N	026 55.9 W	586	7	14	CTD,LADCP,O2
2900	083020	1032	BE	66 00.6 N	026 48.8 W	439	4	12	CTD,LADCP,O2
2900	083020	1053	BO	66 00.6 N	026 48.0 W	439	4	12	CTD,LADCP,O2
2900	083020	1111	EN	66 00.7 N	026 47.4 W	439	4	12	CTD,LADCP,O2
2901	083020	1213	BE	65 56.1 N	026 29.6 W	289	3	10	CTD,LADCP,O2
2901	083020	1226	BO	65 56.1 N	026 29.4 W	289	3	10	CTD,LADCP,O2

2901	090120	1240	EN	65 56.1 N	026 29.4 W	289	3	10	CTD,LADCP,O2
2902	090120	1008	BE	65 02.8 N	012 42.6 W	155	4	6	CTD,LADCP,O2
2902	090120	1017	BO	65 02.8 N	012 42.6 W	155	4	6	CTD,LADCP,O2
2902	090120	1030	EN	65 02.8 N	012 42.6 W	155	4	6	CTD,LADCP,O2
2903	090120	1222	BE	64 49.3 N	012 30.2 W	175	4	7	CTD,LADCP,O2
2903	090120	1234	BO	64 49.2 N	012 30.2 W	175	4	7	CTD,LADCP,O2
2903	090120	1247	EN	64 49.1 N	012 30.2 W	175	4	7	CTD,LADCP,O2
2904	090120	1513	BE	64 38.7 N	012 20.8 W	169	2	7	CTD,LADCP,O2
2904	090120	1523	BO	64 38.7 N	012 20.8 W	169	2	7	CTD,LADCP,O2
2904	090120	1537	EN	64 38.6 N	012 20.9 W	169	2	7	CTD,LADCP,O2
2905	090120	1721	BE	64 27.9 N	012 07.6 W	337	5	10	CTD,LADCP,O2
2905	090120	1733	BO	64 27.9 N	012 07.6 W	337	5	10	CTD,LADCP,O2
2905	090120	1749	EN	64 27.9 N	012 07.6 W	337	5	10	CTD,LADCP,O2
2906	090120	1922	BE	64 19.1 N	011 57.5 W	418	4	12	CTD,LADCP,O2
2906	090120	1940	BO	64 19.2 N	011 57.3 W	418	4	12	CTD,LADCP,O2
2906	090120	1957	EN	64 19.3 N	011 56.8 W	418	4	12	CTD,LADCP,O2
2907	090120	2122	BE	64 11.2 N	011 47.7 W	366	7	10	CTD,LADCP,O2
2907	090120	2150	BO	64 11.5 N	011 46.9 W	366	7	10	CTD,LADCP,O2
2907	090120	2208	EN	64 11.6 N	011 45.5 W	366	7	10	CTD,LADCP,O2
2908	090120	2327	BE	64 02.8 N	011 39.7 W	348	4	11	CTD,LADCP,O2
2908	090120	2343	BO	64 02.7 N	011 39.5 W	348	4	11	CTD,LADCP,O2
2908	090220	2358	EN	64 02.6 N	011 39.2 W	348	4	11	CTD,LADCP,O2
2909	090220	0133	BE	63 52.6 N	011 27.1 W	356	3	11	CTD,LADCP,O2
2909	090220	0145	BO	63 52.6 N	011 27.1 W	356	3	11	CTD,LADCP,O2
2909	090220	0201	EN	63 52.5 N	011 27.6 W	356	3	11	CTD,LADCP,O2
2910	090220	0321	BE	63 44.3 N	011 16.4 W	392	6	11	CTD,LADCP,O2
2910	090220	0334	BO	63 44.2 N	011 16.6 W	392	6	11	CTD,LADCP,O2
2910	090220	0351	EN	63 44.2 N	011 17.1 W	392	6	11	CTD,LADCP,O2
2911	090220	0515	BE	63 36.4 N	011 03.0 W	328	5	11	CTD,LADCP,O2
2911	090220	0528	BO	63 36.4 N	011 02.9 W	328	5	11	CTD,LADCP,O2
2911	090220	0543	EN	63 36.6 N	011 03.0 W	328	5	11	CTD,LADCP,O2
2912	090220	0708	BE	63 28.2 N	010 49.7 W	442	6	13	CTD,LADCP,O2
2912	090220	0722	BO	63 28.2 N	010 49.6 W	442	6	13	CTD,LADCP,O2
2912	090220	0741	EN	63 28.3 N	010 49.6 W	442	6	13	CTD,LADCP,O2
2913	090220	0925	BE	63 20.8 N	010 23.6 W	345	3	11	CTD,LADCP,O2
2913	090220	0940	BO	63 20.8 N	010 23.5 W	345	3	11	CTD,LADCP,O2
2913	090220	0957	EN	63 21.0 N	010 23.2 W	345	3	11	CTD,LADCP,O2
2914	090220	1228	BE	63 13.3 N	010 00.5 W	486	4	13	CTD,LADCP,O2
2914	090220	1244	BO	63 13.2 N	010 00.4 W	486	4	13	CTD,LADCP,O2
2914	090220	1304	EN	63 13.2 N	010 00.4 W	486	4	13	CTD,LADCP,O2
2915	090220	1438	BE	63 06.0 N	009 38.0 W	496	4	12	CTD,LADCP,O2
2915	090220	1454	BO	63 05.9 N	009 38.0 W	496	4	12	CTD,LADCP,O2
2915	090220	1513	EN	63 05.9 N	009 38.1 W	496	4	12	CTD,LADCP,O2
2916	090220	1711	BE	62 57.3 N	009 10.9 W	447	4	13	CTD,LADCP,O2
2916	090220	1726	BO	62 57.3 N	009 10.8 W	447	4	13	CTD,LADCP,O2
2916	090220	1747	EN	62 57.3 N	009 10.8 W	447	4	13	CTD,LADCP,O2
2917	090220	1920	BE	62 51.0 N	008 50.0 W	466	4	13	CTD,LADCP,O2
2917	090220	1937	BO	62 51.1 N	008 49.8 W	466	4	13	CTD,LADCP,O2
2917	090220	1958	EN	62 51.2 N	008 49.6 W	466	4	13	CTD,LADCP,O2
2918	090220	2143	BE	62 43.3 N	008 26.5 W	493	5	13	CTD,LADCP,O2
2918	090220	2159	BO	62 43.3 N	008 26.1 W	493	5	13	CTD,LADCP,O2
2918	090320	2223	EN	62 43.4 N	008 25.3 W	493	5	13	CTD,LADCP,O2
2919	090320	0001	BE	62 34.9 N	008 01.9 W	409	6	10	CTD,LADCP,O2
2919	090320	0015	BO	62 35.0 N	008 01.5 W	409	6	10	CTD,LADCP,O2
2919	090320	0029	EN	62 35.1 N	008 00.9 W	409	6	10	CTD,LADCP,O2

2920	090320	0209	BE	62 26.8 N	007 36.9 W	104	4	5	CTD,LADCP,O2
2920	090320	0217	BO	62 26.7 N	007 36.9 W	104	4	5	CTD,LADCP,O2
2920	090320	0227	EN	62 26.6 N	007 37.0 W	104	4	5	CTD,LADCP,O2
2921	090320	0801	BE	61 52.4 N	007 57.3 W	155	5	6	CTD,LADCP,O2
2921	090320	0812	BO	61 52.4 N	007 57.1 W	155	5	6	CTD,LADCP,O2
2921	090320	0825	EN	61 52.6 N	007 57.0 W	155	5	6	CTD,LADCP,O2
2922	090320	1007	BE	61 42.8 N	008 02.5 W	169	4	7	CTD,LADCP,O2
2922	090320	1017	BO	61 42.9 N	008 02.3 W	169	4	7	CTD,LADCP,O2
2922	090320	1031	EN	61 42.8 N	008 01.8 W	169	4	7	CTD,LADCP,O2
2923	090320	1206	BE	61 33.2 N	008 08.4 W	285	3	10	CTD,LADCP,O2
2923	090320	1219	BO	61 33.1 N	008 08.2 W	285	3	10	CTD,LADCP,O2
2923	090320	1231	EN	61 33.1 N	008 08.0 W	285	3	10	CTD,LADCP,O2
2924	090320	1317	BE	61 28.4 N	008 10.5 W	444	3	12	CTD,LADCP,O2
2924	090320	1334	BO	61 28.2 N	008 10.5 W	444	3	12	CTD,LADCP,O2
2924	090320	1403	EN	61 28.4 N	008 10.4 W	444	3	12	CTD,LADCP,O2
2925	090320	1436	BE	61 25.9 N	008 11.9 W	701	5	16	CTD,LADCP,O2
2925	090320	1454	BO	61 25.7 N	008 12.0 W	701	5	16	CTD,LADCP,O2
2925	090320	1520	EN	61 25.8 N	008 12.0 W	701	5	16	CTD,LADCP,O2
2926	090320	1551	BE	61 23.4 N	008 13.3 W	812	4	16	CTD,LADCP,O2
2926	090320	1616	BO	61 23.2 N	008 13.3 W	812	4	16	CTD,LADCP,O2
2926	090320	1646	EN	61 23.3 N	008 13.4 W	812	4	16	CTD,LADCP,O2
2927	090320	1714	BE	61 20.9 N	008 14.4 W	703	3	13	CTD,LADCP,O2
2927	090320	1734	BO	61 20.8 N	008 14.4 W	703	3	13	CTD,LADCP,O2
2927	090320	1759	EN	61 20.8 N	008 14.4 W	703	3	13	CTD,LADCP,O2
2928	090320	1826	BE	61 18.5 N	008 15.4 W	493	3	12	CTD,LADCP,O2
2928	090320	1843	BO	61 18.4 N	008 15.5 W	493	3	12	CTD,LADCP,O2
2928	090320	1903	EN	61 18.3 N	008 15.5 W	493	3	12	CTD,LADCP,O2
2929	090320	2246	BE	61 03.9 N	008 23.3 W	99	3	6	CTD,LADCP,O2
2929	090320	2258	BO	61 03.9 N	008 23.4 W	99	3	6	CTD,LADCP,O2
2929	090420	2310	EN	61 03.9 N	008 23.2 W	99	3	6	CTD,LADCP,O2
2930	090420	0156	BE	60 44.5 N	008 34.7 W	205	6	8	CTD,LADCP,O2
2930	090420	0207	BO	60 44.5 N	008 34.8 W	205	6	8	CTD,LADCP,O2
2930	090420	0217	EN	60 44.3 N	008 35.0 W	205	6	8	CTD,LADCP,O2
2931	090420	0506	BE	60 25.3 N	008 46.4 W	397	5	11	CTD,LADCP,O2
2931	090420	0520	BO	60 25.3 N	008 46.5 W	397	5	11	CTD,LADCP,O2
2931	090420	0535	EN	60 25.3 N	008 46.5 W	397	5	11	CTD,LADCP,O2
2932	090420	0711	BE	60 15.8 N	008 51.9 W	944	9	17	CTD,LADCP,O2
2932	090420	0736	BO	60 15.8 N	008 52.0 W	944	9	17	CTD,LADCP,O2
2932	090420	0805	EN	60 15.8 N	008 51.7 W	944	9	17	CTD,LADCP,O2
2933	090420	0945	BE	60 06.2 N	008 57.7 W	1198	6	19	CTD,LADCP,O2
2933	090420	1017	BO	60 06.2 N	008 57.7 W	1198	6	19	CTD,LADCP,O2
2933	090420	1054	EN	60 06.1 N	008 57.6 W	1198	6	19	CTD,LADCP,O2
2934	090420	1223	BE	59 56.6 N	009 03.2 W	1362	4	19	CTD,LADCP,O2
2934	090420	1253	BO	59 56.5 N	009 03.5 W	1362	4	19	CTD,LADCP,O2
2934	090420	1334	EN	59 56.6 N	009 03.7 W	1362	4	19	CTD,LADCP,O2
2935	090420	1456	BE	59 47.0 N	009 09.0 W	1378	3	19	CTD,LADCP,O2
2935	090420	1526	BO	59 46.9 N	009 09.3 W	1378	3	19	CTD,LADCP,O2
2935	090420	1606	EN	59 46.9 N	009 09.4 W	1378	3	19	CTD,LADCP,O2
2936	090420	1715	BE	59 38.6 N	009 13.9 W	1431	3	19	CTD,LADCP,O2
2936	090420	1748	BO	59 38.4 N	009 14.1 W	1431	3	19	CTD,LADCP,O2
2936	090420	1830	EN	59 38.4 N	009 14.2 W	1431	3	19	CTD,LADCP,O2
2937	090420	1941	BE	59 30.0 N	009 19.9 W	1461	9	21	CTD,LADCP,O2
2937	090420	2014	BO	59 30.0 N	009 19.9 W	1461	9	21	CTD,LADCP,O2
2937	090520	2056	EN	59 30.1 N	009 19.4 W	1461	9	21	CTD,LADCP,O2
2938	090520	1751	BE	61 42.4 N	005 57.6 W	298	2	8	CTD,LADCP,O2

2938	090520	1805	BO	61 42.5 N	005 57.7 W	298	2	8	CTD,LADCP,O2
2938	090520	1816	EN	61 42.5 N	005 57.8 W	298	2	8	CTD,LADCP,O2
2939	090520	1940	BE	61 36.3 N	005 37.2 W	320	5	10	CTD,LADCP,O2
2939	090520	1953	BO	61 36.3 N	005 37.3 W	320	5	10	CTD,LADCP,O2
2939	090520	2008	EN	61 36.3 N	005 37.3 W	320	5	10	CTD,LADCP,O2
2940	090520	2124	BE	61 31.0 N	005 18.8 W	291	5	10	CTD,LADCP,O2
2940	090520	2139	BO	61 30.9 N	005 18.9 W	291	5	10	CTD,LADCP,O2
2940	090520	2153	EN	61 31.0 N	005 18.9 W	291	5	10	CTD,LADCP,O2
2941	090520	2305	BE	61 25.5 N	005 00.5 W	228	3	8	CTD,LADCP,O2
2941	090520	2320	BO	61 25.4 N	005 00.7 W	228	3	8	CTD,LADCP,O2
2941	090620	2331	EN	61 25.4 N	005 00.7 W	228	3	8	CTD,LADCP,O2
2942	090620	0043	BE	61 20.0 N	004 43.0 W	741	6	14	CTD,LADCP,O2
2942	090620	0104	BO	61 19.9 N	004 42.9 W	741	6	14	CTD,LADCP,O2
2942	090620	0126	EN	61 19.9 N	004 42.9 W	741	6	14	CTD,LADCP,O2
2943	090620	0225	BE	61 15.5 N	004 29.5 W	1052	5	15	CTD,LADCP,O2
2943	090620	0250	BO	61 15.5 N	004 29.4 W	1052	5	15	CTD,LADCP,O2
2943	090620	0318	EN	61 15.4 N	004 29.6 W	1052	5	15	CTD,LADCP,O2
2944	090620	0414	BE	61 11.9 N	004 18.0 W	1082	4	16	CTD,LADCP,O2
2944	090620	0445	BO	61 11.6 N	004 18.8 W	1082	4	16	CTD,LADCP,O2
2944	090620	0516	EN	61 11.3 N	004 19.8 W	1082	4	16	CTD,LADCP,O2
2945	090620	0626	BE	61 08.0 N	004 04.1 W	1122	4	19	CTD,LADCP,O2
2945	090620	0651	BO	61 07.9 N	004 04.7 W	1122	4	19	CTD,LADCP,O2
2945	090620	0724	EN	61 07.8 N	004 05.6 W	1122	4	19	CTD,LADCP,O2
2946	090620	0832	BE	61 04.0 N	003 52.0 W	1153	5	21	CTD,LADCP,O2
2946	090620	0858	BO	61 04.2 N	003 52.4 W	1153	5	21	CTD,LADCP,O2
2946	090620	0939	EN	61 04.6 N	003 53.0 W	1153	5	21	CTD,LADCP,O2
2947	090620	1053	BE	60 59.0 N	003 37.9 W	1107	4	20	CTD,LADCP,O2
2947	090620	1117	BO	60 59.0 N	003 38.0 W	1107	4	20	CTD,LADCP,O2
2947	090620	1153	EN	60 59.3 N	003 38.4 W	1107	4	20	CTD,LADCP,O2
2948	090620	1319	BE	60 51.9 N	003 17.8 W	684	4	18	CTD,LADCP,O2
2948	090620	1338	BO	60 51.9 N	003 18.0 W	684	4	18	CTD,LADCP,O2
2948	090620	1405	EN	60 51.9 N	003 18.0 W	684	4	18	CTD,LADCP,O2
2949	090620	1535	BE	60 45.0 N	002 54.8 W	356	4	11	CTD,LADCP,O2
2949	090620	1549	BO	60 44.9 N	002 55.0 W	356	4	11	CTD,LADCP,O2
2949	090620	1604	EN	60 44.9 N	002 55.0 W	356	4	11	CTD,LADCP,O2
2950	090620	1727	BE	60 38.0 N	002 35.9 W	134	4	6	CTD,LADCP,O2
2950	090620	1737	BO	60 37.9 N	002 35.9 W	134	4	6	CTD,LADCP,O2
2950	090620	1748	EN	60 37.9 N	002 35.9 W	134	4	6	CTD,LADCP,O2
2951	090620	1913	BE	60 31.1 N	002 16.1 W	143	4	7	CTD,LADCP,O2
2951	090620	1923	BO	60 31.0 N	002 15.9 W	143	4	7	CTD,LADCP,O2
2951	090620	1936	EN	60 30.9 N	002 16.0 W	143	4	7	CTD,LADCP,O2

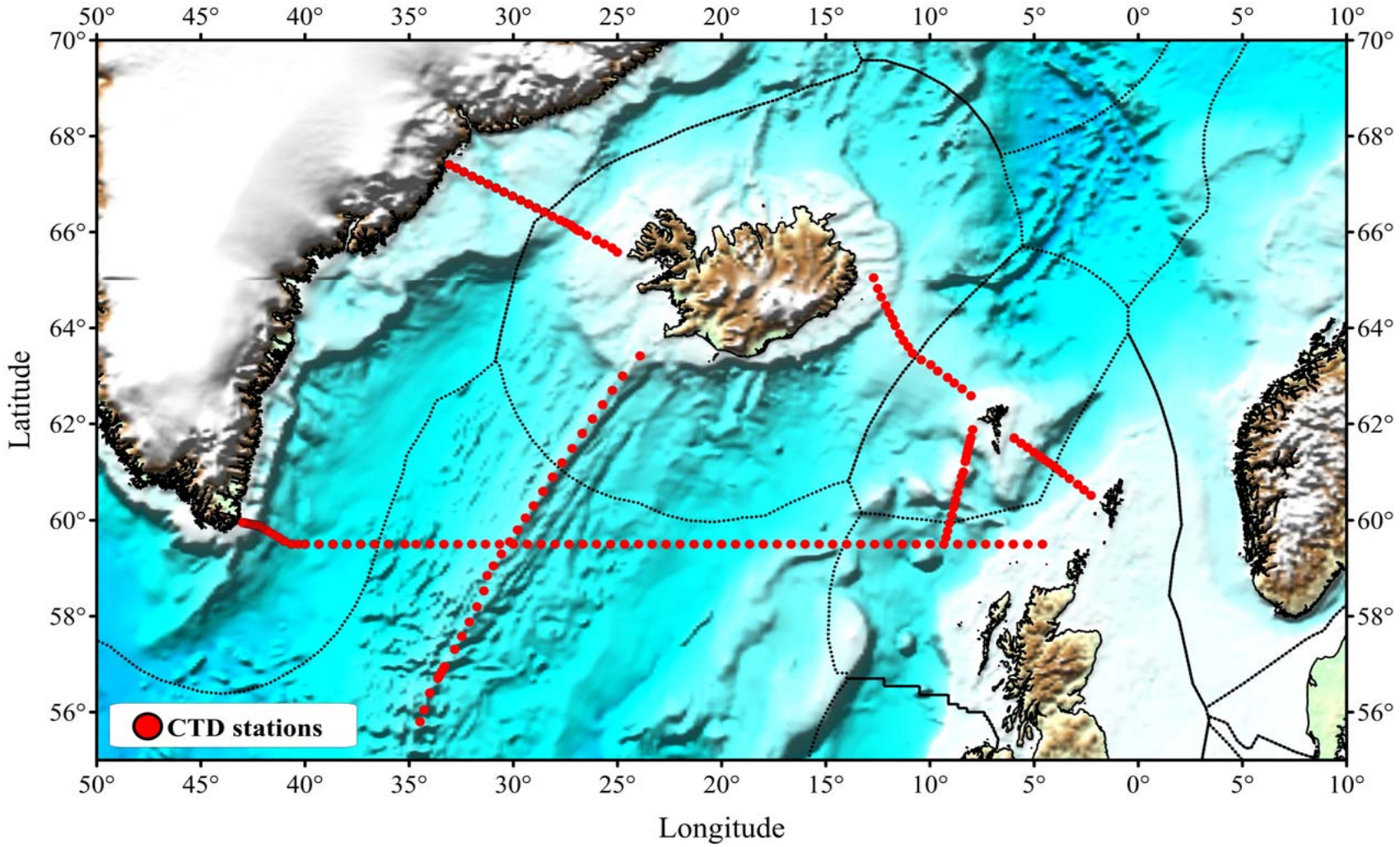

Fig. 1 Station locations (red circles)

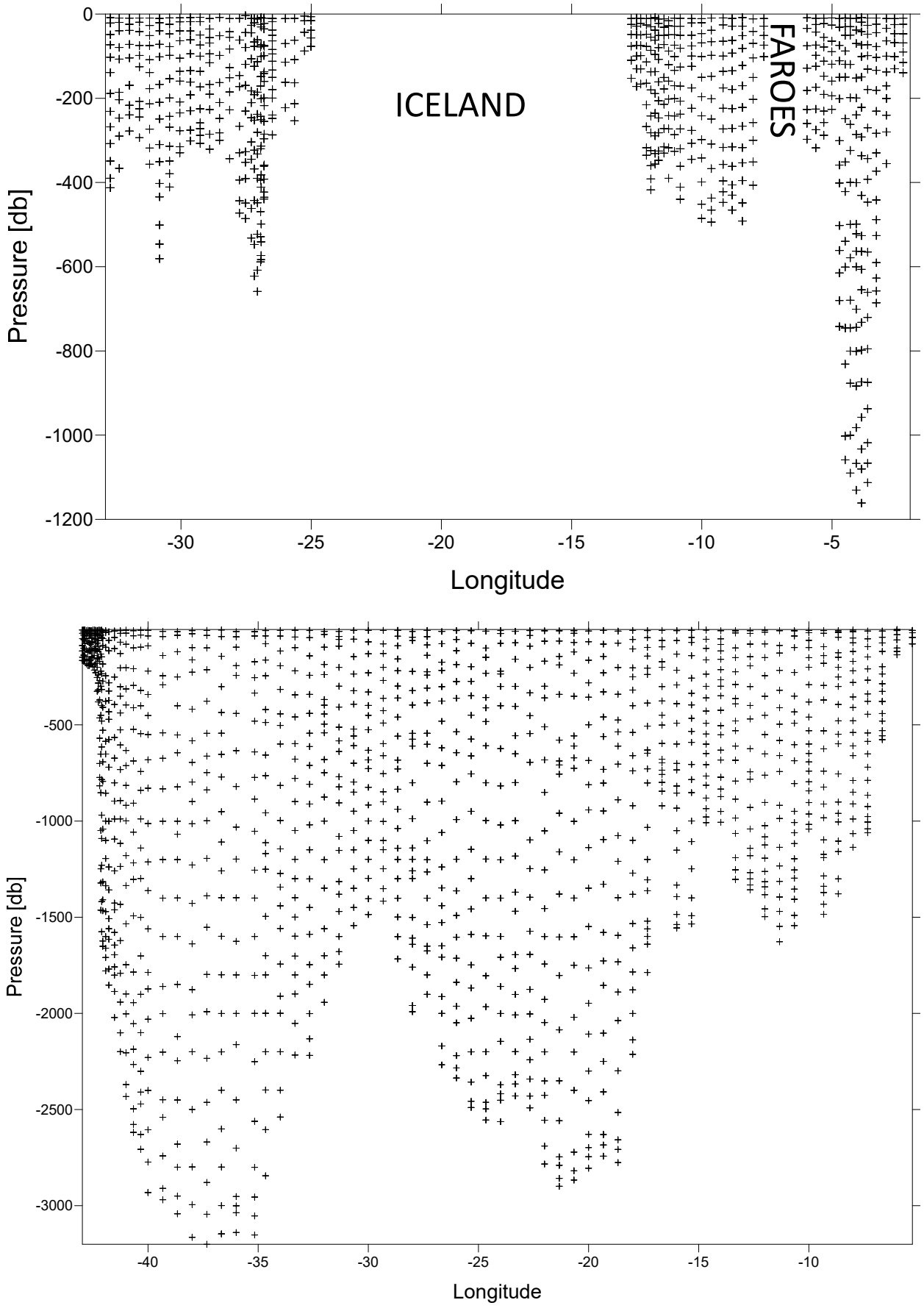

Figure 2. Vertical distribution of oxygen samples along (a) sill section (b) the 59.5 section.

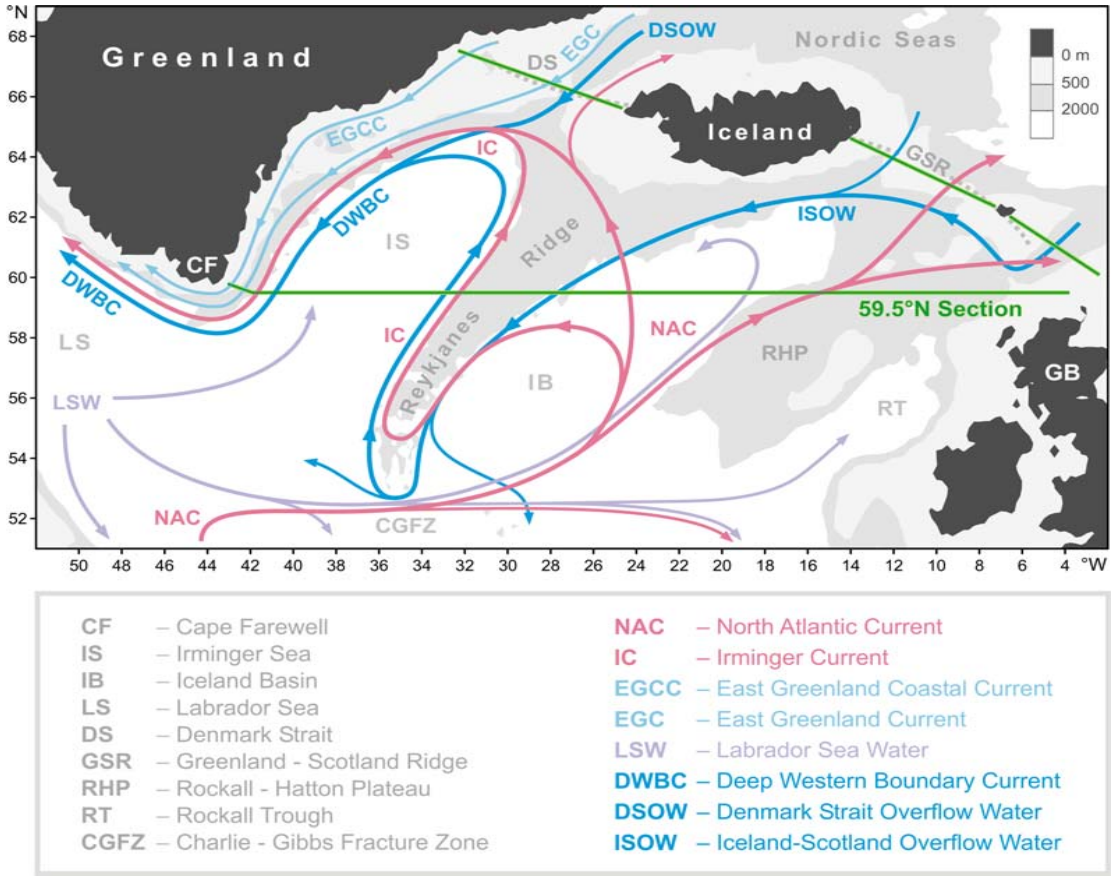

Figure 3. Schematic diagram of the large-scale circulation in the northern North Atlantic compiled from [Schmitz and McCartney, 1993; Schott and Brandt, 2007; Sutherland and Pickart, 2008; Lherminier et al., 2010]. Abbreviations for the main topographic features, currents and water masses are explained in the legend. The nominal locations of the 59.5°N hydrographic section (1997 – present) and sections across the straits between Greenland, Iceland, Faeroe and Shetland Islands (2011 – present) are shown with the solid green lines.

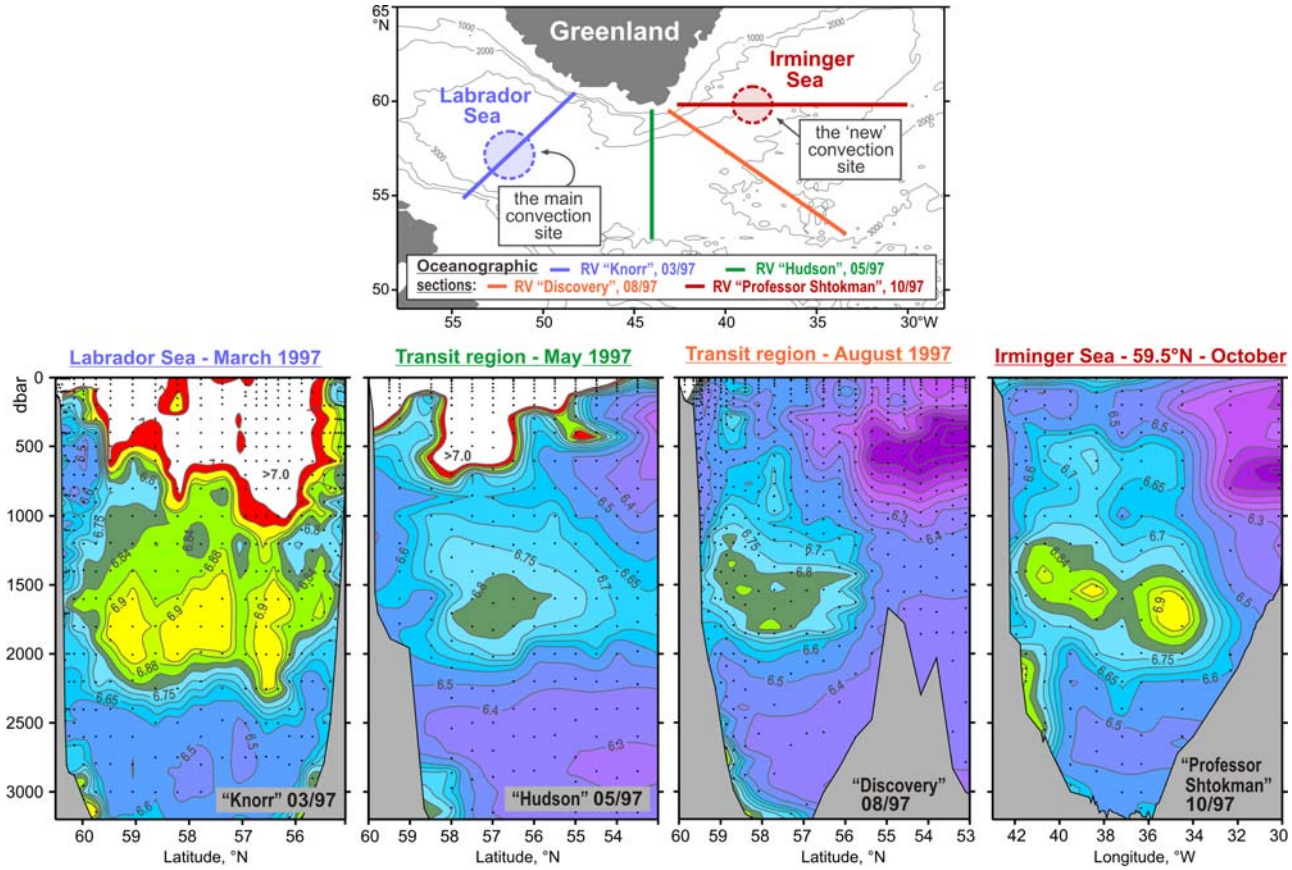

Figure 4. Oxygen concentrations (ml/l) in the water column (lower panel) as observed in March–October 1997 in four hydrographic sections (upper panel) ending nearby the southern tip of Greenland. A separate oxygen maximum in the LSW layer (1000–2000 m) in the Irminger Sea at 59.5°N strongly implies local convective renewal of LSW before 1997. Adapted from [Falina et al., 2007].

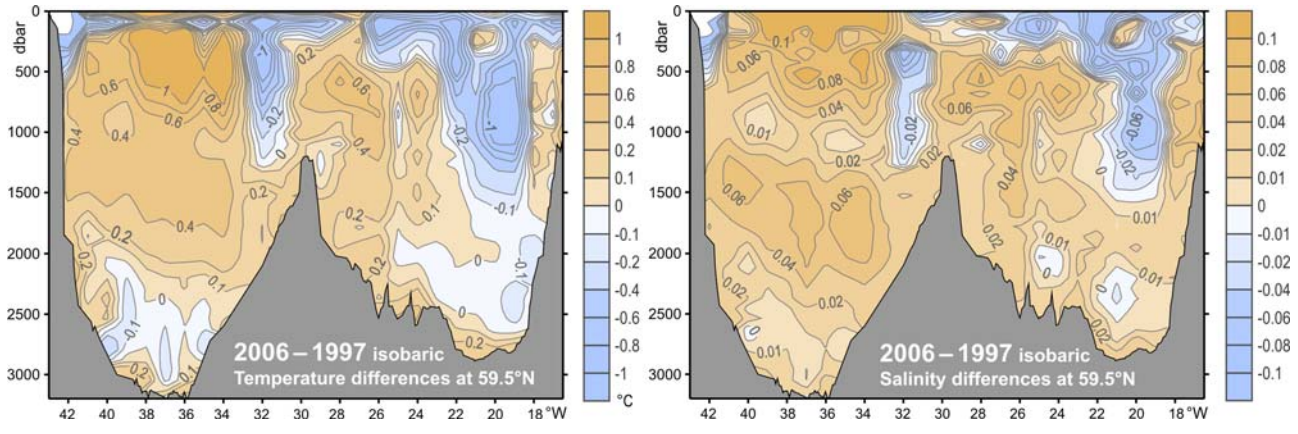

Figure 5. Warming and salinification in the northern North Atlantic between the mid-1990s and mid-2000s, as observed at 59.5°N. The figure shows the 2006–1997 temperature (°C, left) and salinity (right) differences on isobaric surfaces in the Irminger Sea and Iceland Basin. Adapted from [Sarafanov et al., 2007].

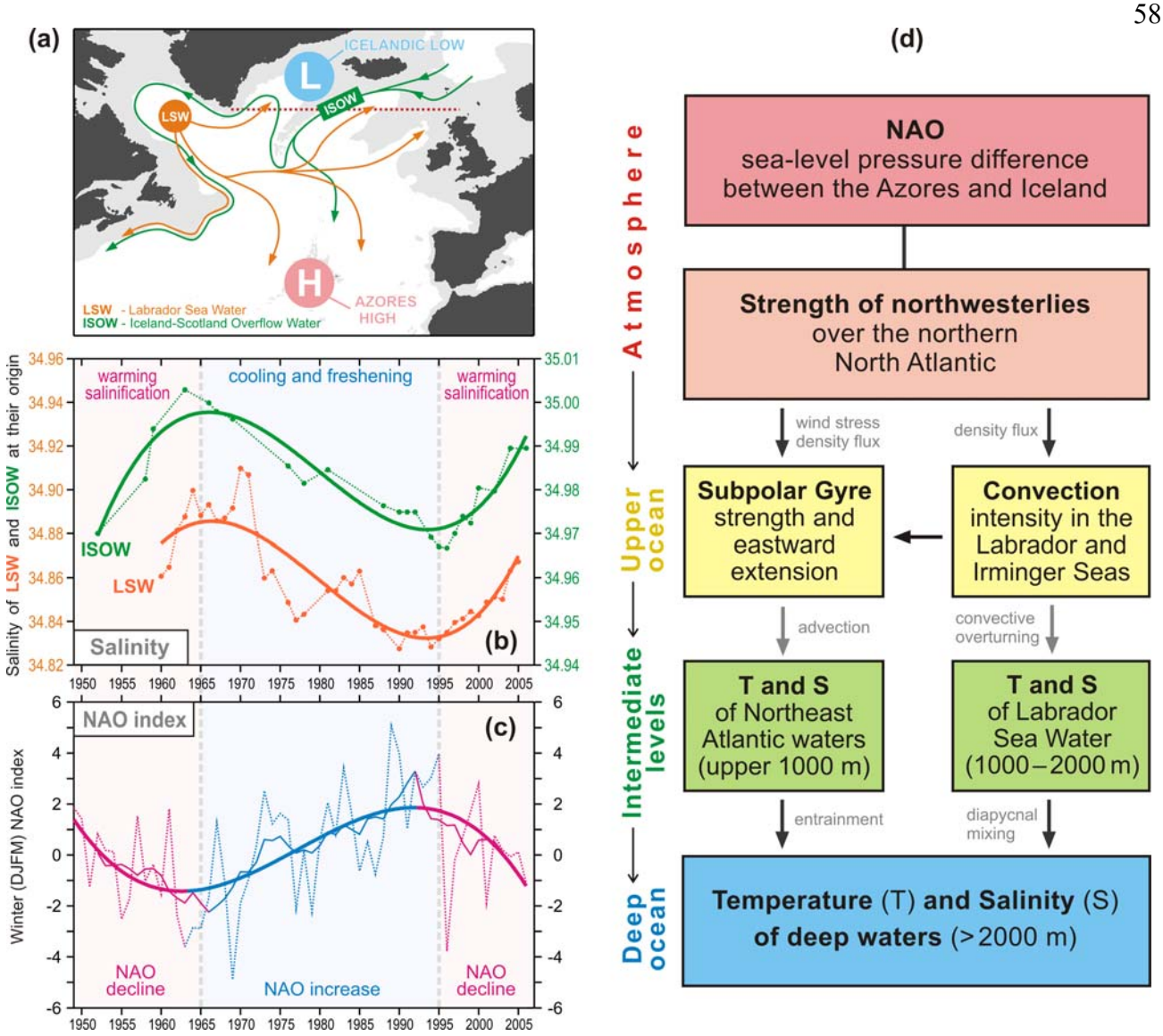

Figure 6. Coherence of the decadal salinity changes (1950s – 2000s) of the intermediate (LSW) and deep (ISOW) waters in the northern North Atlantic and their link to the North Atlantic Oscillation (NAO) index. **(a)** Schematic representation of the LSW and ISOW pathways and locations of the Icelandic Low (L) and Azores High (H) centers constituting the NAO dipole pattern. The red dotted line indicates the 59.5°N transatlantic section. **(b)** Salinity time series for LSW in the Labrador Sea [Yashayaev, 2007] and ISOW in the Iceland basin [Boessenkool et al., 2007; Sarafanov et al., 2007] overlaid by the third order polynomial fits. **(c)** Time series of the winter NAO index, after [Hurrell, 1995], overlaid by 7-year running mean and third order polynomial fit. **(d)** Mechanism of the NAO effect on the decadal changes in temperature (T) and salinity (S) of the northern North Atlantic intermediate and deep waters. Positive / negative links shown with the dark / light grey arrows mean that changes in 'causative' and 'consequential' characteristics have the same / opposite sign(s). The overall effect of the NAO on T and S of the in the water column is negative: persistent NAO decline leads to warming and salinification of the water masses and vice versa, as shown in (b) and (c). Adapted from [Sarafanov, 2009].

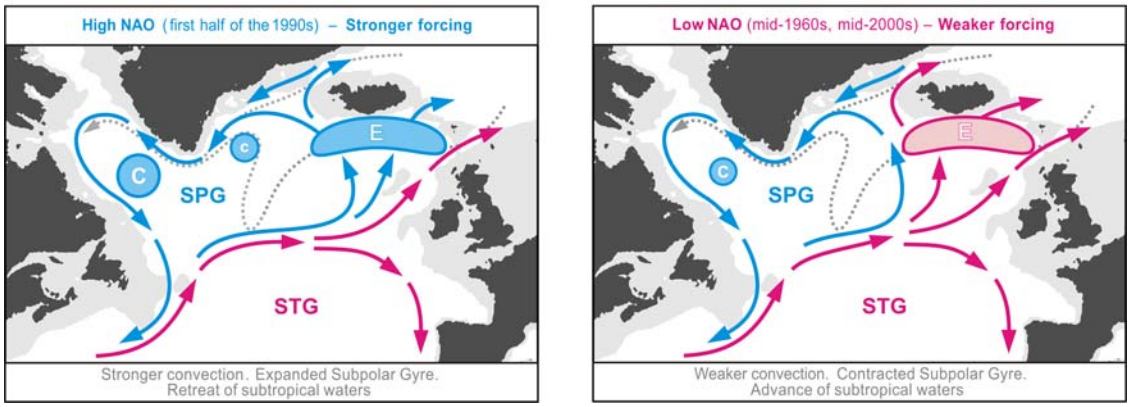

Figure 7. Schematic representation of the upper-ocean circulation and convection intensity in the northern North Atlantic under high (left) and low (right) NAO conditions. Blue (magenta) solid arrows indicate the upper-ocean flows with higher fraction of colder fresher subpolar (warmer saltier subtropical) waters. The main pathways of the Nordic overflow-derived deep waters are shown with the dotted curves. "C" and "E" symbols are used to denote, respectively, the deep convection sites and the domain, where the Atlantic waters are entrained into ISOW. Larger (smaller) circles indicate stronger (weaker) convection. SPG and STG – the subpolar and subtropical gyres, respectively. Adapted from [Sarafanov, 2009].

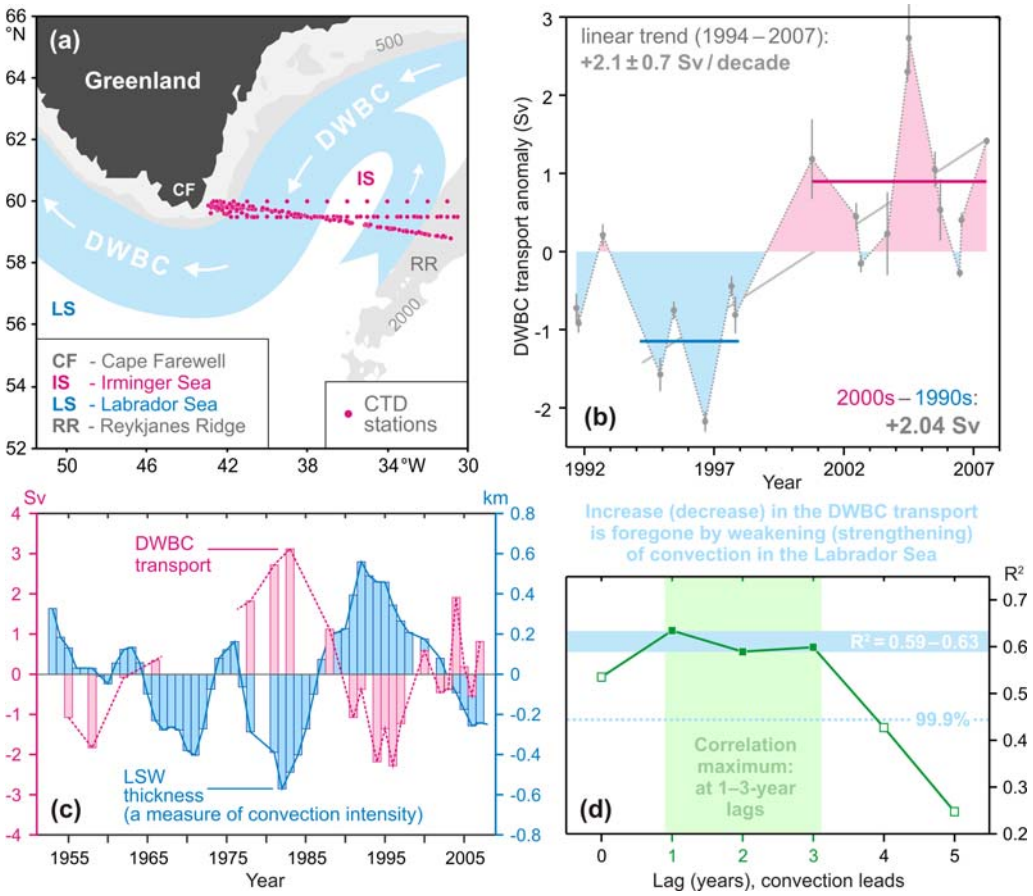

Figure 8. The Deep Western Boundary Current (DWBC) transport variability and its link to the convection intensity in the Labrador Sea. **(a)** Locations of the hydrographic sections (1991–2007) and schematic of the deep water circulation in the Irminger Sea. **(b)** The DWBC transport anomalies at Cape Farewell in 1991–2007, 1 Sv = 10^6 m^3 s^{-1}. The 1994–1997 and 2000–2007 mean anomalies and the 1994–2007 linear trend are shown. **(c)** Anomalies of the DWBC transport at Cape Farewell and the Labrador Sea Water (LSW) thickness in the Labrador Sea in the 1950s–2000s. **(d)** Correlation coefficient (R^2) for the two times series shown in **(c)** at the 0–5-year lag, the LSW thickness leads. The correlation maximum is achieved at the 1–3-year lag. The DWBC transport anomalies in the southern Irminger Sea are foregone by the convection intensity anomalies in the Labrador Sea. Adapted from [Sarafanov et al., 2009].

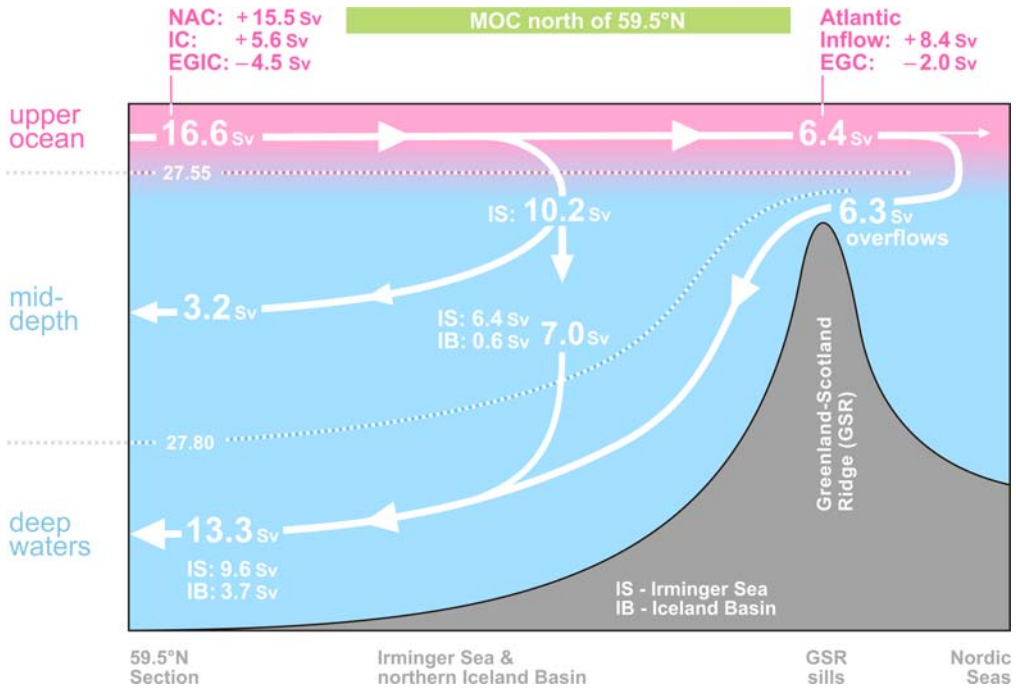

Figure 9. Schematic diagram of the Meridional Overturning Circulation (MOC) at the northern periphery of the Atlantic Ocean, northeast of Cape Farewell. The dotted lines refer to the σ_0 isopycnals 27.55 and 27.80. The arrows denote the integral meridional and diapycnal volume fluxes. Where the signs are specified, the positive (negative) transports are northward (southward). The NAC and EGIC transports in the upper layer ($\sigma_0 < 27.55$) at 59.5°N are the throughputs accounting for the recirculations. EGIC – the East Greenland / Irminger Current – refers to the upper part of the Western Boundary Current. Other abbreviations are explained in the legend to **Figure 3**. Adapted from [Sarafanov et al., 2012].

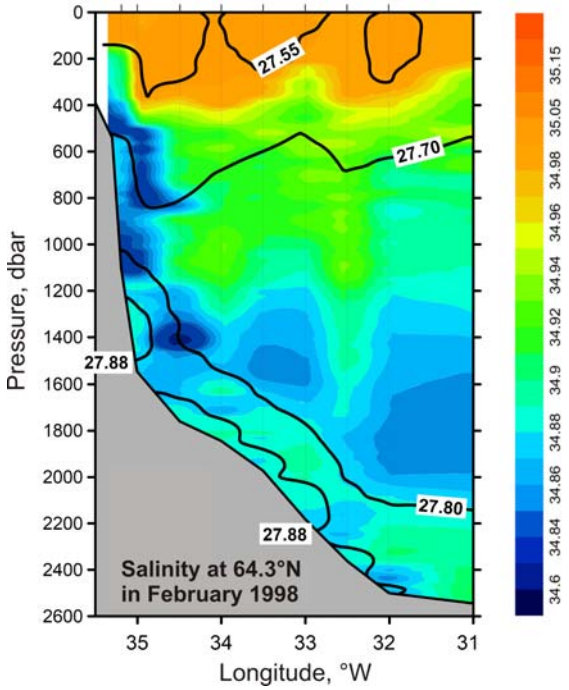

Figure 10. Salinity observed in the northwestern Irminger Sea at 64.3°N in February 1998. The σ_0 isopycnals 27.55, 27.70, 27.80 and 27.88 are plotted as the thick black lines; the station locations are marked with the ticks on the top axis. The plot shows fresh dense waters descending (cascading) down the continental slope of Greenland down to the LSW layer ($27.70 < \sigma_0 < 27.80$) and the layer of the Nordic Seas overflow-derived deep waters ($\sigma_0 > 27.80$). Adapted from [Falina et al., 2012].

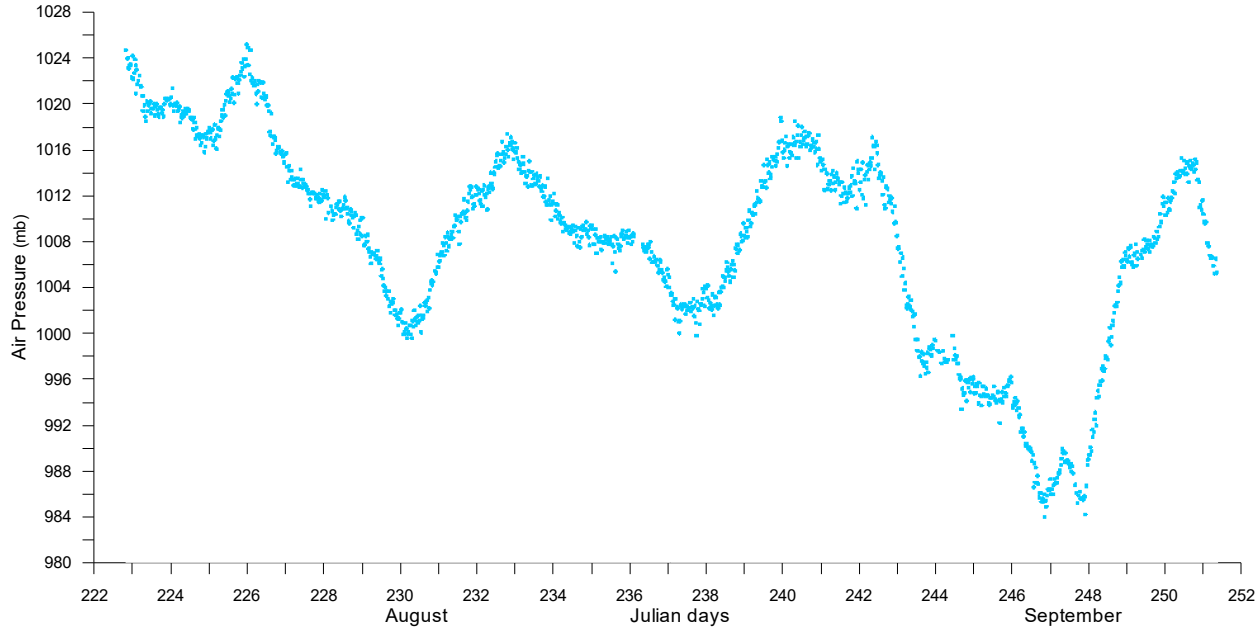

Figure 11. 3-minute atmospheric pressure (mb) measured during 50 cruise of Akademik Sergey Vavilov.

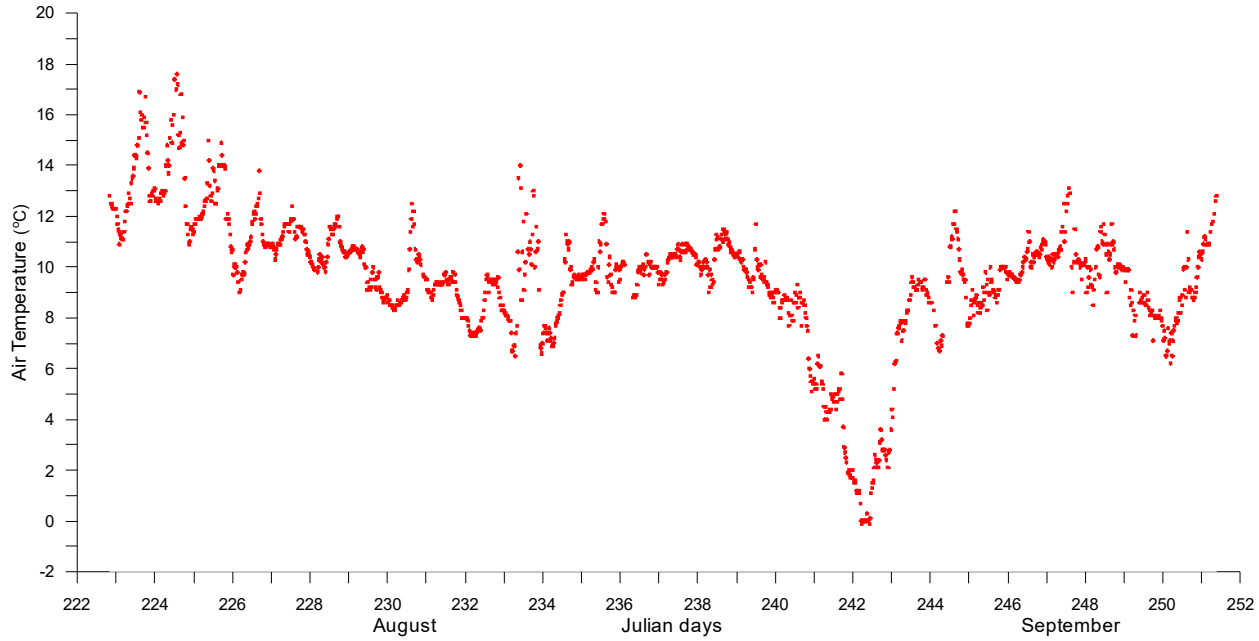

Figure 12. 3-minute Air temperature (°C) measured during 50 cruise of Akademik Sergey Vavilov.

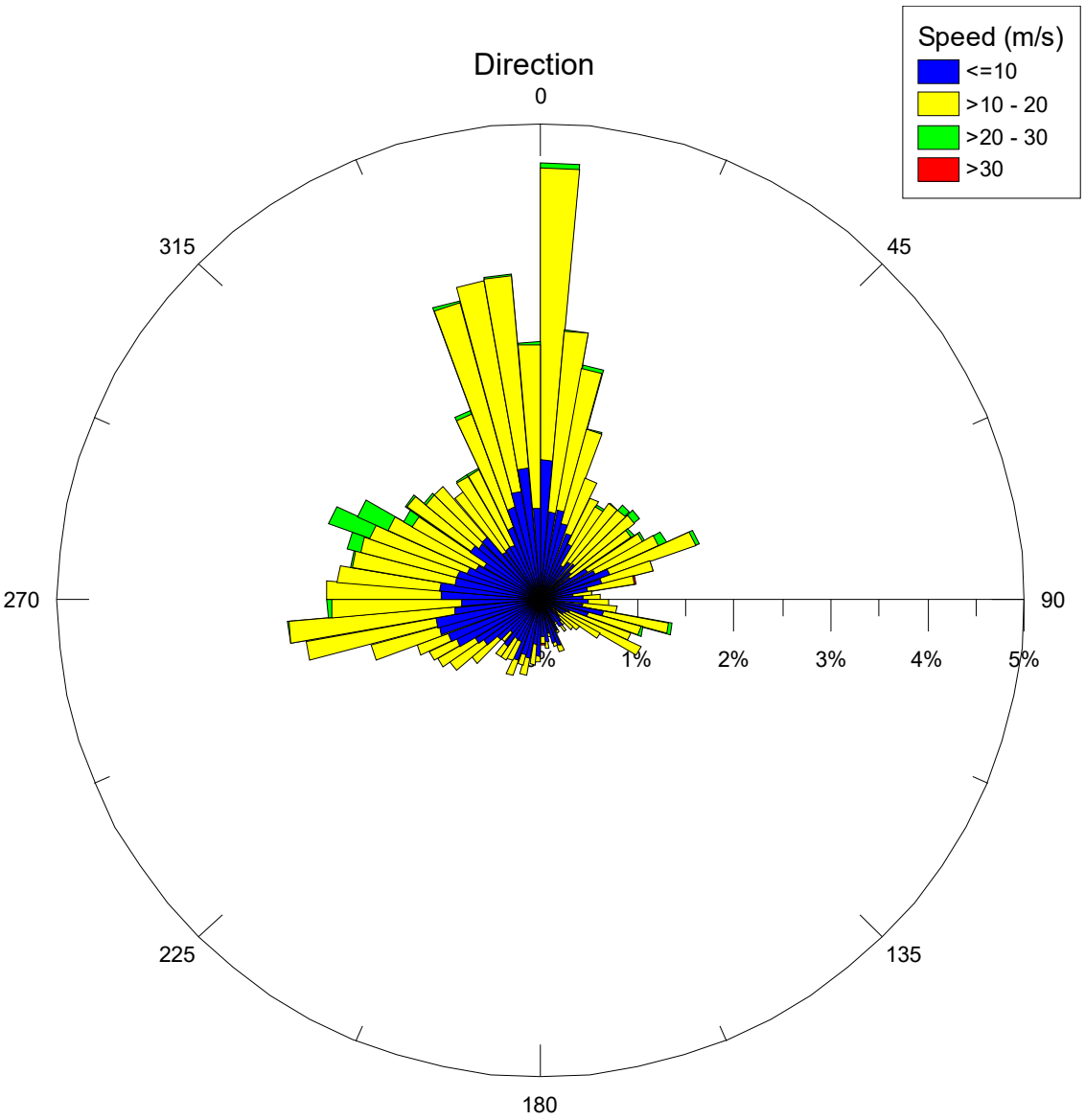

Figure 13. Wind speed (m/s) and direction (^{o}) measured during 50 cruise of Akademik Sergey Vavilov.

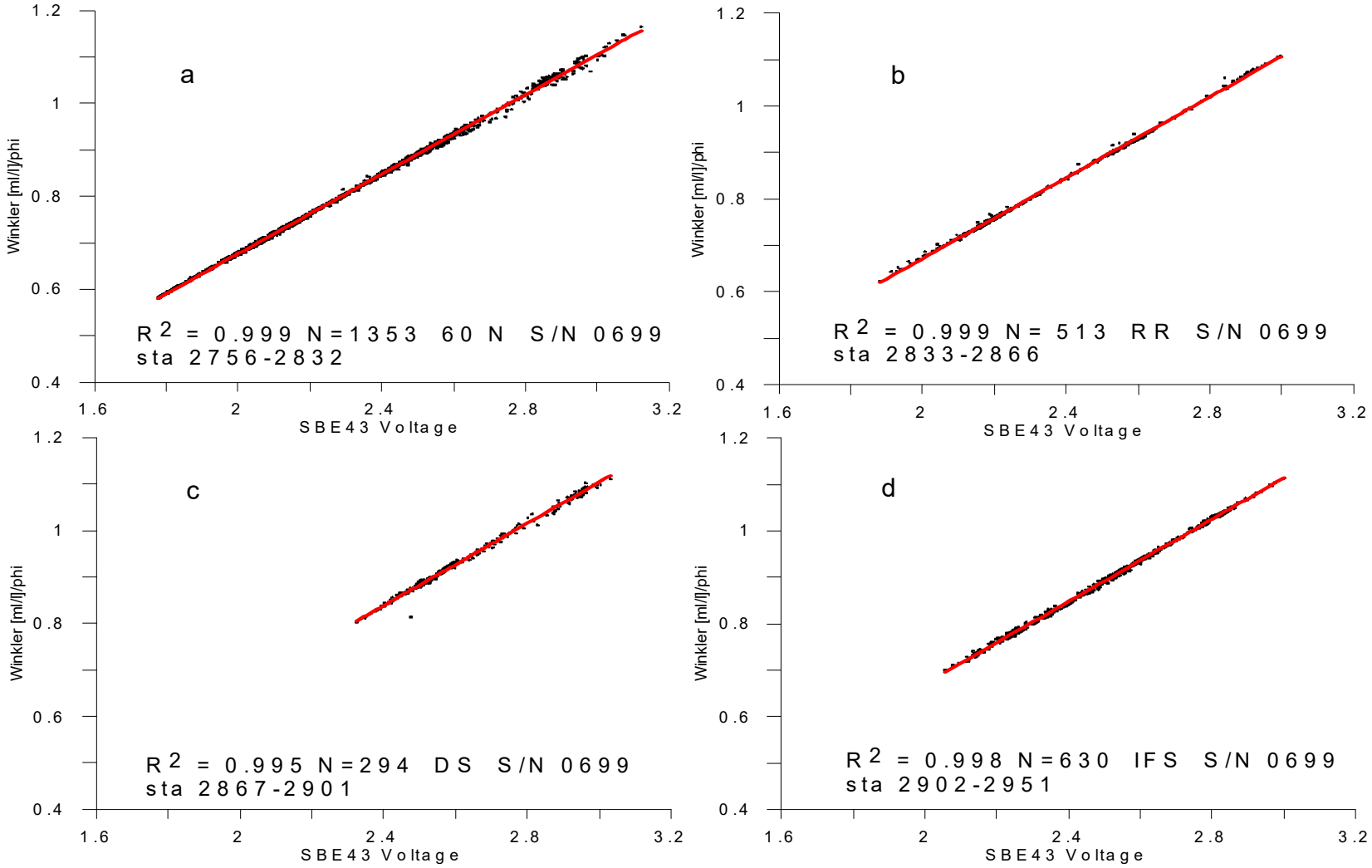

Figure 14 Regression lines for Winkler oxygen divided by φ versus SBE 43 output voltage for (a) 59.5 transatlantic section, (b) RR section, (c) DS section, and (d) IFS sections. Oxygen data collected at the East Greenland shelf is regressed separately.

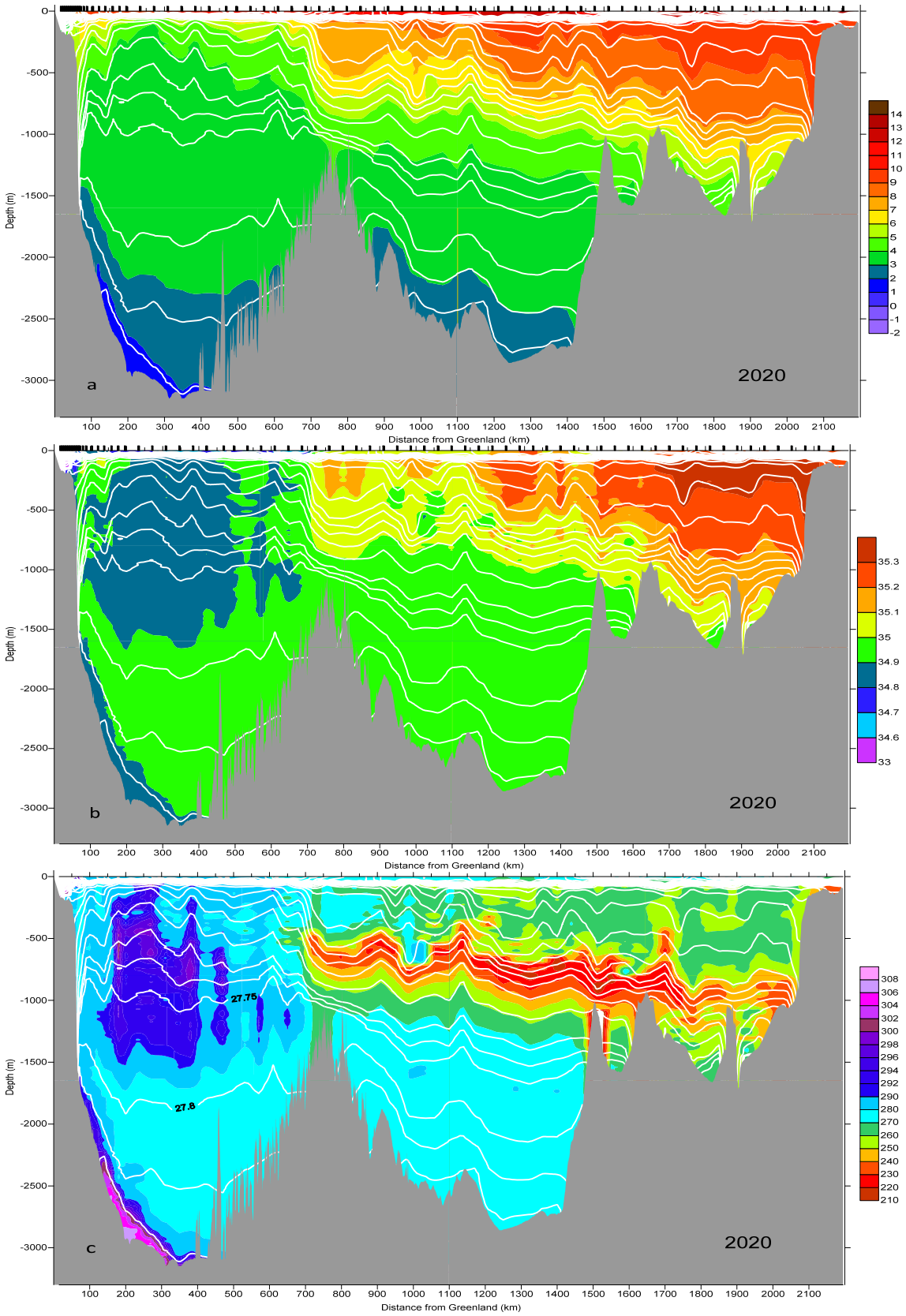

Figure 15 The vertical distribution of (a) potential temperature (°C) and (b) salinity (c) dissolved oxygen (µmol/kg) along 59.5 N in 10-20August 2020. Potential density is shown in white. Station position is shown by vertical marks.

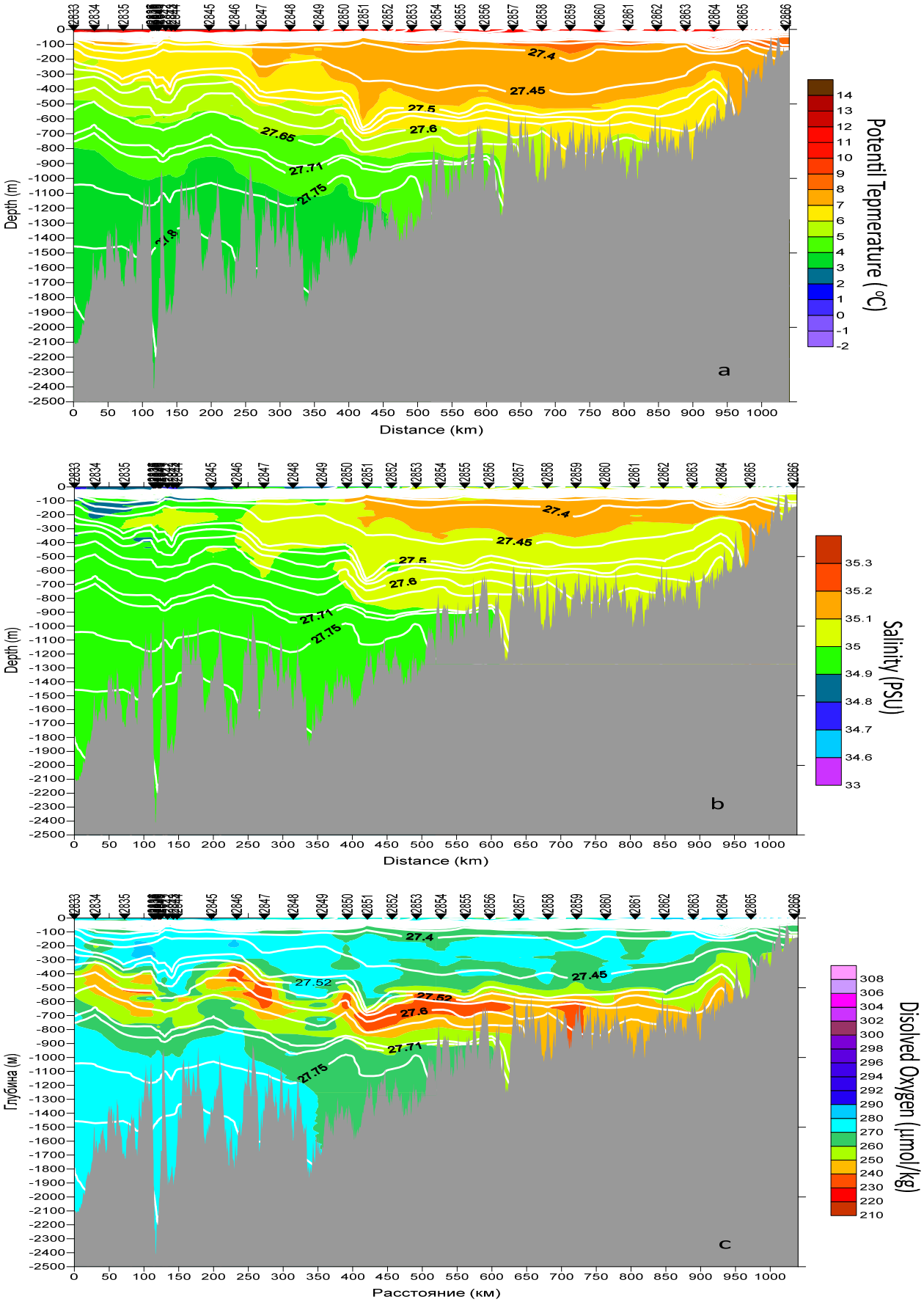

Figure 16. The vertical distribution of (a) potential temperature (°C) and (b) salinity (c) dissolved oxygen (µmol/kg) along northern Reykjanes Ridge crest in 22-26 August 2020. Potential density is shown in white. Station position is shown by vertical marks

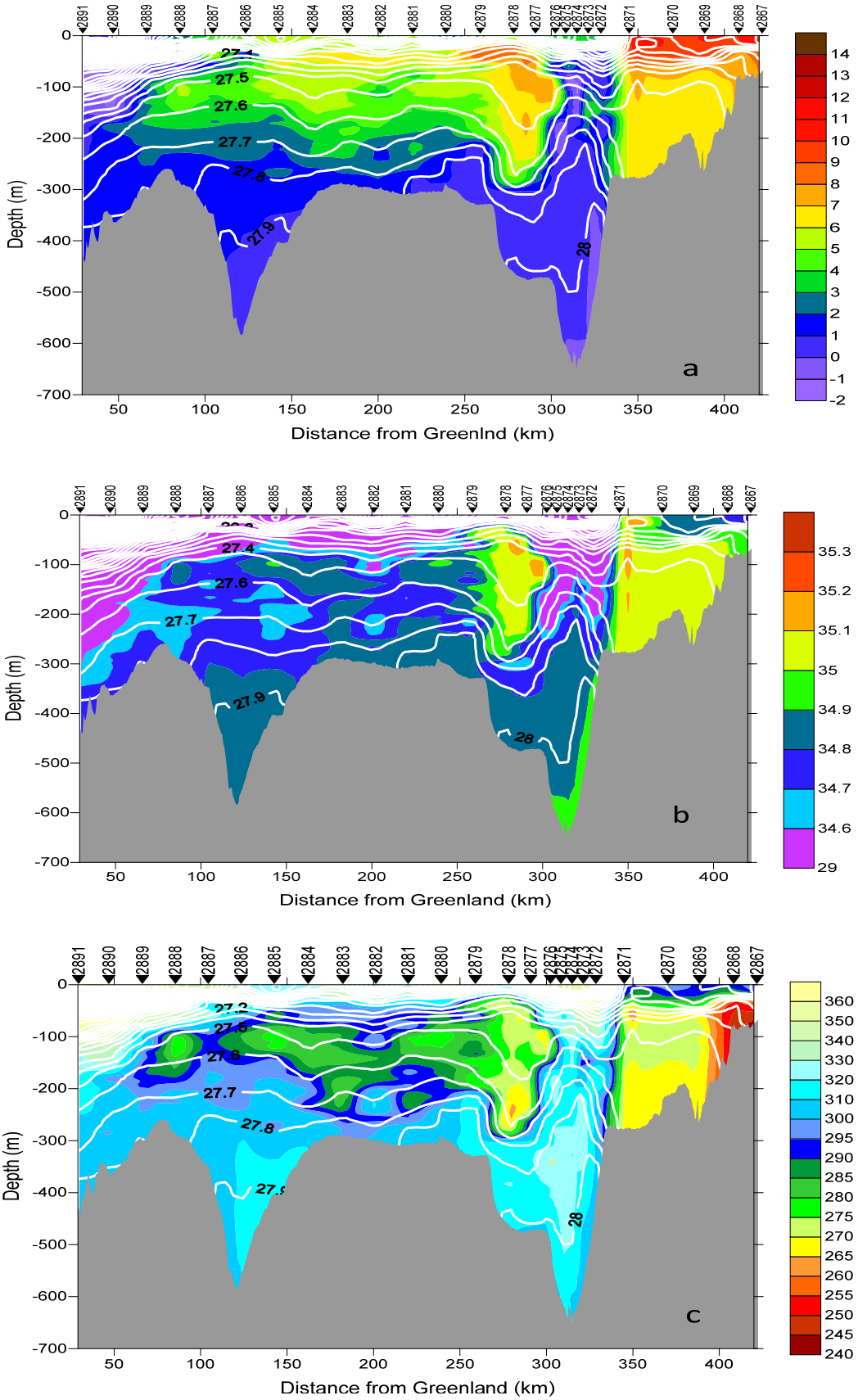

Figure 17. The vertical distribution of (a) potential temperature (°C) and (b) salinity (c) dissolved oxygen (μmol/kg) across Denmark Strait in 27-30 August 2020. Potential density is shown in white. Station position is shown by vertical marks

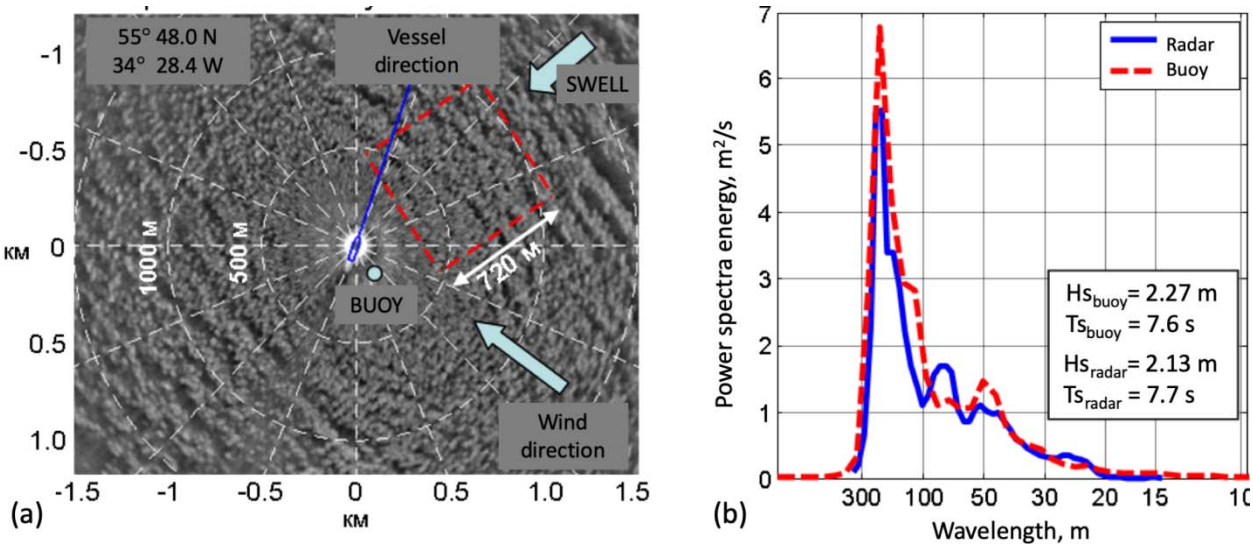

Figure 18. (a) Fragment of the radar image at station No. 2833 (22 Aug 2020 15:38 UTC), north is at the top, the outline in the center and the line show the current orientation of the vessel, the red box indicates the area of the radar signal processing. (b) Comparison of the non-directional frequency spectrum *E(f)* from the radar and buoy data for the station.

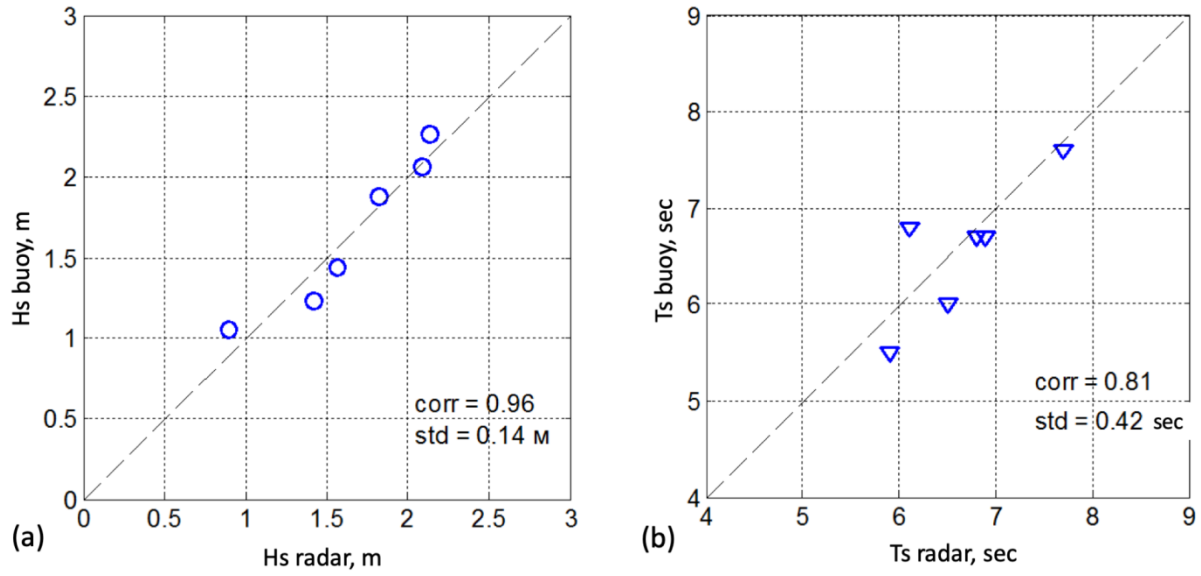

Figure 19. (a) Comparison of the significant wave height and (b) the period of energy-carrying waves for 6 stations